UNCLASSIFIED

AD 277 479

Reproduced
by the

ARMED SERVICES TECHNICAL INFORMATION AGENCY
ARLINGTON HALL STATION
ARLINGTON 12, VIRGINIA

UNCLASSIFIED

AFCRL-62-341

STUDIES IN IONOSPHERIC PROPAGATION

PART I -- The Exact Earth-Flattening Procedure in Ionospheric

Propagation Problems

by

M. Katzin   and   B. Y.-C. Koo

PART II -- VLF Signal Enhancements and HF Fadeouts During

Sudden Ionospheric Disturbances

by

M. Katzin

Report No. CRC-7233-1 $62-4-1$
15 April 1962

ELECTROMAGNETIC RESEARCH CORPORATION

5001 COLLEGE AVENUE
COLLEGE PARK, MD.

STUDIES IN IONOSPHERIC PROPAGATION

PART I -- The Exact Earth-Flattening Procedure in Ionospheric

Propagation Problems

by

M. Katzin   and   B. Y.-C. Koo

PART II -- VLF Signal Enhancements and HF Fadeouts During

Sudden Ionospheric Disturbances

by

M. Katzin

Final Report
on
Contract AF19(604)-7233

Project 5631
Task 563109

Prepared for

ELECTRONICS RESEARCH DIRECTORATE
AIR FORCE CAMBRIDGE RESEARCH LABORATORIES
OFFICE OF AEROSPACE RESEARCH
UNITED STATES AIR FORCE
BEDFORD, MASSACHUSETTS

ELECTROMAGNETIC RESEARCH CORPORATION

5001 COLLEGE AVENUE
COLLEGE PARK, MD.
Report No. CRC-7233-1
15 April 1962

Requests for additional copies by Agencies of the
Department of Defense, their contractors, and other
Government agencies should be directed to the

     Armed Services Technical Information Agency
     Arlington Hall Station
     Arlington 12, Virginia

Department of Defense contractors must be established
for ASTIA service or have their "need-to-know" certi-
fied by the cognizant military agency of their project
or contract.

All other persons and organization should apply to the

     U.S. Department of Commerce
     Office of Technical Services
     Washington 25, D.C.

THE EXACT EARTH-FLATTENING PROCEDURE IN

IONOSPHERIC PROPAGATION PROBLEMS

ABSTRACT

The exact earth-flattening procedure previously developed for an iso-
tropic spherically-stratified atmosphere, is extended to the case of a
spherical earth and atmosphere enveloped by a sharply bounded ionosphere. The
general solution of the problem is formulated as an integral representation,
from which may be derived either a ray-optical series or a normal mode series.
In the latter case, the normal modes involve the normalized spherical Hankel
function and its derivative. An improved method of obtaining the zeros of
these functions is derived which is not of asymptotic character.

A spheroidal geometry is investigated as a basis for dealing with problems
of non-spherical stratification. Solutions for the angular function as an
infinite series of Bessel functions are found, of the same type as in the
spherical case. The radial function is expressed as a sum of the normalized
spherical Hankel function and its derivative, the coefficients of these func-
tions being infinite series in terms of powers of the ratio of semi-focal
distance to radius. It is shown that the zeros of the radial function as a
function of order, which are required for the normal mode solution, may be
found by the same procedure that was developed for the spherical case

PART II

VLF ENHANCEMENTS AND HF FADEOUTS DURING

SUDDEN IONOSPHERIC DISTURBANCES

ABSTRACT

Simultaneous observations of short-wave fade-outs of a 13.5-Mc/s signal and sudden signal enhancements of a 31.15-kc/s signal over substantially the same transatlantic path of approximately 5400 km show no evident correlation between the magnitudes of the two effects of the SID. This absence of correlation is understandable on the basis of a two-layer D-region.

The relative intensifications of the two D-regions will depend on the spectral distribution of hard X-rays in the 1-10 A range emitted during a flare, which can be expected to vary from flare to flare. Since the increase in h-f absorption is the sum of the increases in the two regions, while the v-l-f enhancement is occasioned only by the changes at the lower level, no correlation should result between the two effects.

On the other hand, an adequate explanation of the mechanism of the v-l-f enhancement is not available on the basis of present knowledge. Phase measurements show that a definite decrease in height of the lower boundary of the D-region is caused by the flare. This reduced height causes reflection to take place at a level of higher collision frequency, which should result in a decrease in the effective conductivity of the layer if the ionization gradient remains the same. Consequently, it appears that an increase in the sharpness of the lower boundary of the D-region is required during the onset of a solar flare. The mechanism by which this takes place needs to be determined.

Table of Contents

THE EXACT EARTH-FLATTENING PROCEDURE IN

IONOSPHERIC PROPAGATION PROBLEMS

1. INTRODUCTION

In an earlier paper [1]*, an exact earth-flattening procedure was given for propagation in an inhomogeneous atmosphere over a spherical earth. This formulation led to the realization of the physical nature of the approximations introduced by the usual earth-flattening procedure. In particular it was shown that the differential equation for the height-gain function in the usual earth-flattening approximation was equivalent to a small change in the refractive index variation with height. In other words, the physical problem is changed somewhat by the earth-flattening approximation. The amount of this change or deviation increases with height, but should not be of great consequence in problems of tropospheric propagation.

In the case of ionospheric propagation, the important heights involved (in wavelengths) may be considerably greater. Consequently, it appeared desirable to investigate whether the exact earth-flattening procedure could improve ionospheric propagation analysis. This is one objective of the research conducted under this part of the contract, and is accomplished in Sec. 2. An additional objective is the extension of this theory to take into account lateral variations of the refractive index (non-horizontal stratification). For this purpose a spheroidal geometry is considered. This is carried out in Sec. 3.

The subject of ionospheric propagation, involving complex layer distributions, magneto-ionic splitting and propagation at arbitrary angles to the earth's magnetic field, coupling between modes, etc., encompasses many ramifications which probably never will be capable of a complete self-contained treatment. Consequently, for

---

*Numbers in brackets refer to the corresponding numbers in the References on p. 29.

purposes of the present study we shall adopt an often-used idealization of the ionosphere in order to confine attention to the specific objectives stated above. For this purpose the ionosphere will be considered to be sharply bounded and of uniform electrical properties. This assumption is the one usually made in studying v-l-f ionospheric propagation, so that the results will be of chief interest in this frequency range. It is then logical to consider only a vertical dipole source, since this is the only effective form of radiator at these frequencies.

2. SPHERICALLY-STRATIFIED IONOSPHERE

A rigorous formulation of the field due to a vertical electric or magnetic dipole in an inhomogeneous isotropic atmosphere over a spherical earth was given by Friedman [2]. For plane geometry, this was extended by Wait [3] to include the essential mixed polarization effects due to the anisotropy of a sharply bounded ionosphere. For completeness, a rigorous formulation of the spherical problem (with a sharp ionosphere boundary) will be sketched here. This formulation will be given in a form adapted to direct introduction of the earth-flattening procedure.

In the isotropic case treated by Friedman, it is possible to formulate separately the cases of vertical electric and vertical magnetic dipole sources, corresponding to vertically and horizontally polarized fields, respectively. In each case, the various field components are derivable from a Hertz vector whose direction is radial. Actually this Hertz vector (within an appropriate multiplying factor) is nothing more than the radial component of the electric (magnetic) field in the case of the radial electric (magnetic) dipole source, since all other components are derivable from the radial components (see, for example, Schelkunoff [4]). In the anisotropic case, however, electric and magnetic modes are coupled in the ionosphere,

2

so that the problem must be formulated in terms of mixed components from the outset.

2.1 Formulation of the Problem

The geometry of the problem is shown in Fig. 1. A vertical dipole of (infinitesimal) length l and current I is located at $R = b$, the boundaries of
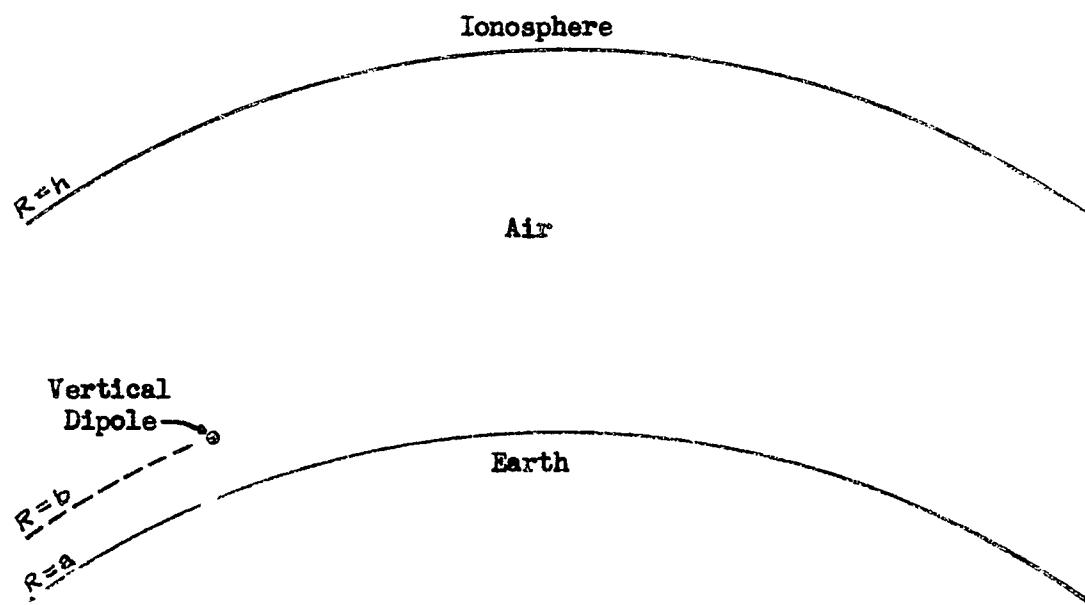
Fig. 1 - Geometry of spherical earth, with concentric sharply-bounded spherical ionosphere, excited by dipole source.

earth and ionosphere being at $R = a$ and $R = h$, respectively.

Consideration of the physics of the problem will assist a proper formulation. Thus, the primary field due to the source will give rise to a field which has a polarization determined by the direction of the source current. This primary field, in turn, will give rise to reflected components at the boundaries of the earth and ionosphere. The ionosphere will introduce magneto-ionic splitting, so that new

polarization components will arise there. From these facts it is clear that a combination of electric and magnetic Hertz vectors must be used for derivation of the fields. The two components, in general, will differ in amplitude and phase, so that we must represent the radial Hertz vector by a column matrix of the form

$$[\underset{\sim}{\Pi}] = \begin{bmatrix} \Pi_e \\ \Pi_m \end{bmatrix} = \begin{bmatrix} \Pi_e \\ \Pi_m \end{bmatrix} \underset{\sim}{i}_R \tag{2.1}$$

where $\underset{\sim}{i}_R$ is the unit radial vector, and the subscripts e and m refer to electric and magnetic modes, respectively.

Consider first the electric component Π_e and write it as the sum of a primary and a secondary field

$$\Pi_e = \Pi_1 + \Pi_3. \tag{2.2}$$

Now put

$$\Pi_j = \omega \mu \underset{\sim}{R} P_j. \tag{2.3}$$

Π_1 is stimulated by the vertical source current, while Π_3 arises from reflection at the boundaries. Then the corresponding fields are derivable from the equations

$$E_e = k \underset{\sim}{R}(P_1 + P_3) + \frac{1}{k^2} \, grad \left[\frac{\partial}{\partial R} \left\{ R(P_1 + P_3) \right\} \right], \tag{2.4}$$

$$H_e = \frac{i}{\omega \mu} \, curl \left[k \underset{\sim}{R}(P_1 + P_3) \right], \tag{2.5}$$

providing that P_1 is a solution of the inhomogeneous reduced wave equation

$$\nabla^2 P_1 + k^2 P_1 = \frac{i \omega \mu}{kR} J_i \tag{2.6}$$

and P_3 is a solution of the homogeneous equation

$$\nabla^2 P_3 + k^2 P_3 = 0. \tag{2.7}$$

4

First consider (2.6). The current density J_{λ} may be related to the dipole moment $I\ell$ by integrating over the source region:

$$I\ell = \int J_{\lambda}\,dv = \int_{o}^{\infty}\int_{o}^{2\pi}\int_{o}^{\pi} J_{\lambda} R^2 \sin\theta\,d\theta\,d\varphi\,dR,$$

so that

$$J_{\lambda} = \frac{I\ell}{2\pi R^2 \sin\theta}\,\delta(\theta)\delta(R-b). \tag{2.8}$$

Since the right-hand side of (2.6), in virtue of (2.8), is zero everywhere outside the point $(b,0,0)$, the solutions of (2.6) can be assembled from solutions of the corresponding homogeneous equation

$$\nabla^2 P_1 + k^2 P_1 = 0. \tag{2.9}$$

Hence we can separate P_1 in the form

$$R P_1 = T(\theta)\,U_1(R)\,V(\varphi) \tag{2.10}$$

where T, U, and V are functions only of θ, R, and φ, respectively. (2.9) then separates into the equations

$$\frac{d^2 T}{d\theta^2} + \cot\theta\,\frac{dT}{d\theta} + \left(s^2 - \frac{m^2}{\sin^2\theta}\right)T = 0, \tag{2.11}$$

$$\frac{d^2 U_1}{dR^2} + \left(k^2 - \frac{s^2}{R^2}\right)U_1 = 0, \tag{2.12}$$

$$\frac{d^2 V}{d\varphi^2} + m^2 V = 0, \tag{2.13}$$

in which s and π are the separation constants, which as yet are arbitrary, and ultimately will be fixed by the boundary conditions. The various solutions of (2.9) are characterized by different values of s and m, including, possibly, complex values.

We take m to be an integer in order that V have 2π-periodicity in φ, and write the solution of (2.13) in the form

$$V_m = \cos(m\varphi + \gamma_m). \tag{2.14}$$

5

Consequently all solutions of (2.9) with 2π-periodicity in φ may be obtained from the representation

$$R P_i = \sum_{m=0}^{\infty} \int_C A(s)\, T(\theta)\, U_i(R)\, V_m(\varphi)\, ds, \tag{2.15}$$

where the amplitude function $A(s)$ and the path C in the complex s-plane are as yet unspecified. In general, C will extend over an infinite range. $A(s)$ and C may be determined by integrating (2.6) around an infinitesimal region enclosing the dipole source. It can be shown that $A(s) = s$ and $\int_C = \int_0^{\infty}$, provided that $T(0) = 1$, so that

$$R P_i = \sum_{m=0}^{\infty} \int_0^{\infty} s\, T\, U_i V_m\, ds, \tag{2.16}$$

where T is a solution of (2.11), U_1 is a solution of (2.12), and V_m is given by (2.14).

2.2 The Angular Function T

In [1] it was shown that a solution of (2.11) for $m = 0$ is

$$T = \sum_{n=0}^{\infty} s^{-2n} T_{2n}, \tag{2.17}$$

where

$$T_{2n} = \sum_{\nu=0}^{n-1} a_{n,\nu}\, (s\theta)^{2n-\nu}\, Z_{2n-\nu}(s\theta),$$

in which $Z_q(s\theta)$ is a cylinder function. In order that (2.17) have the property $T(0) = 1$ as required, we must choose the cylinder function to be the Bessel function $J_q(s\theta)$, and $a_{0,0} = 1$. Consequently the required solution of (2.11) for $m = 0$ may be written as

$$T = \sum_{n=0}^{\infty} a_n\, (s\theta)^n\, J_n(s\theta). \tag{2.18}$$

It may be shown that a lower bound for the absolute convergence of (2.18) is $|\theta| = 2$, so that this covers a sector greater than $\pm\, \pi/2$.

We now extend this type of solution to the case $m \neq 0$.

Introducing the new independent variable

$$x = s\theta, \tag{2.19}$$

6

and denoting the dependent variable by y, (2.11) becomes

$$y'' + \frac{1}{x}\cot\theta\, y' + \left(1 - \frac{m^2}{s^2\sin^2\theta}\right)y = 0. \tag{2.20}$$

We write (2.20) in the form

$$L(y) \equiv y'' + \frac{1}{x}y' + \left(1 - \frac{m^2}{x^2}\right)y = \left[\frac{1}{x} - \frac{1}{s}\cot\left(\frac{x}{s}\right)\right]y' - m^2\left[\frac{1}{x^2} - \frac{1}{s^2}\csc^2\left(\frac{x}{s}\right)\right]y$$

$$= \sum_{\mu=1}^{\infty} a_\mu\left[\frac{1}{x}y' + (2\mu-1)\frac{m^2}{x^2}y\right]\left(\frac{x}{s}\right)^{2\mu}, \tag{2.21}$$

where

$$a_\mu = 2^{2\mu} B_\mu / (2\mu)! \,, \tag{2.22}$$

the B_μ being the Bernouilli numbers.

Assuming a solution of (2.21) of the form

$$y = \sum_{\nu=0}^{\infty} s^{-2\nu} y_{2\nu}, \tag{2.23}$$

we obtain

$$L(y) = \sum_{\nu=0}^{\infty} s^{-2\nu} L(y_{2\nu}) = \sum_{\nu=0}^{\infty}\sum_{\mu=1}^{\infty} s^{-2(\nu+\mu)} a_\mu x^{2\mu}\left[x^{-1}y'_{2\nu} + (2\mu-1)m^2 x^{-2} y_{2\nu}\right]. \tag{2.24}$$

By equating coefficients of like powers of s, we obtain the system of equations

$$L(y_0) = 0,$$

$$L(y_2) = a_1(x y'_0 + m^2 y_0),$$

$$\cdot\quad\cdot\quad\cdot\quad\cdot\quad\cdot\quad\cdot$$

$$L(y_{2\nu}) = \sum_{\lambda=0}^{\nu-1} a_{\nu-\lambda}\left[x^{2\nu-2\lambda-1} y'_{2\nu} + (2\nu-2\lambda-1)m^2 x^{2\nu-2\lambda-2} y_{2\lambda}\right].$$

A solution of the first equation is

$$y_0 = Z_m(x),$$

where Z_m is any cylinder function. The second equation then becomes

$$L(y_2) = a_1(x Z'_m + m^2 Z_m)$$

$$= a_1[m(m+1)Z_m - x Z_{m+1}] \tag{2.25}$$

By introducing the function

$$C_{m,n}(x) = x^n Z_{m+n}(x), \tag{2.26}$$

which has the property

$$L[C_{m,n}(x)] = 2n\, C_{m,m-1}(x), \tag{2.27}$$

(2.25) becomes

$$L(y_2) = a_1[m(m+1)C_{m,0}-C_{m,1}].$$

Now using the property (2.27), the solution of this equation is seen to be

$$y_2 = a_1\left[\frac{m(m+1)}{2}C_{m,0} - \frac{1}{4}C_{m,1}\right]. \tag{2.28}$$

By induction, we infer that

$$y_{2\nu} = \sum_{q=0}^{\nu}\alpha_{\nu,q}C_{m,\nu+q}. \tag{2.29}$$

Hence the solution of (2.21) should be expressible in the form

$$y = \sum_{n=0}^{\infty}A_n C_{m,n}(x) = \sum_{n=0}^{\infty}A_n (s\theta)^n Z_{m+n}(s\theta) \tag{2.30}$$

The following recursion formulas for $C_{m,n}$ are easily obtained from the

recursion formulas for the cylinder functions:

$$x^{-1}C'_{m,n} = x^{-2}\left[(m+2n)C_{m,n} - C_{m,n+1}\right], \tag{2.31}$$

$$x^{2\lambda}C_{m,n} = \sum_{p=0}^{\lambda}c_{n,\lambda,p}\,C_{m,n+\lambda+p}, \tag{2.32}$$

where

$$c_{n,\lambda,p} = (-)^p\frac{\lambda!\,(m+n+\lambda)!\,2^{\lambda-p}}{p!\,(\lambda-p)!\,(m+n+p)!}. \tag{2.33}$$

If we substitute (2.30) into (2.23), and use (2.31) and (2.32) to eliminate

powers of x on the right-hand side, we obtain

$$\sum_{n=0}^{\infty}2(n+1)A_{n+1}C_{m,n} = \sum_{p=0}^{\infty}\sum_{\mu=0}^{\infty}\sum_{j=0}^{\mu}A_p\,a_{\mu+1}s^{-2(\mu+1)}\left(D\,c_{p,\mu,j}\,C_{m,p+\mu+j} - c_{p+1,\mu,j}\,C_{m,p+\mu+j+1}\right),$$

where

$$A_0 = 1,$$

$$D = (2\mu+1)m^2 + m + 2p.$$

By equating coefficients of like orders of the function $C_{m,n}$ on the two sides of

this equation, we obtain the recursion formula

$$A_{n+1} = \frac{1}{2(n+1)}\left\{\sum_{p=0}^{n}\sum_{\mu=\frac{n-p}{2}}^{n-p}D\,c_{p,\mu,n-p-\mu} - \sum_{p=0}^{n-1}\sum_{\mu=\frac{n-p-1}{2}}^{n-p-1}c_{p+1,\mu,n-p-\mu-1}\right\}A_p\,a_{\mu+1}s^{-2(\mu+1)}. \tag{2.34}$$

Consequently, the required solution of (2.11) is

$$T = \sum_{n=0}^{\infty}A_n(s\theta)^n J_{m+n}(s\theta). \tag{2.35}$$

8

The advantage of using an expansion for T in terms of Bessel functions, instead of the standard expression in terms of the associated Legendre functions, is that a more accurate calculation is possible than by the use of the asymptotic expansion for the latter functions.

2.3 The Radial Function U

With T as given by (2.35) the solution of (2.9) is

$$RP_1 = \sum_{m=0}^{\infty} \sum_{n=0}^{\infty} \int_0^{\infty} A_n (s\theta)^n J_{m+n} (s\theta) \cos(m\varphi + \gamma_m) U_1 \, s \, ds, \tag{2.36}$$

where $A_0 = 1$ and A_n is given by the (2.34).

The integral along the positive real s-axis in (2.36) may be transformed into an integral along the entire real axis in the following way:

Write

$$J_{m+n}(s\theta) = \tfrac{1}{2}\left[H_{m+n}^{(1)}(s\theta) + H_{m+n}^{(2)}(s\theta) \right] = \tfrac{1}{2}\left[H_{m+n}^{(2)}(s\theta) - e^{-(m+n)\pi i} H_{m+n}^{(2)}(s\theta e^{-i\pi}) \right],$$

and note from (2.11) and (2.12) that T and U are even functions of s. In the integral corresponding to $H_{m+n}^{(2)}(s\theta e^{-i\pi})$ make the substitution $s' = s e^{-i\pi}$, whereupon the integral for that term becomes

$$\tfrac{1}{2} \int_{-\infty}^{0} \cdots H_{m+n}^{(2)}(s\theta) \, s \, ds$$

in view of the fact that the integrand is an even function of s. Then (2.36) becomes

$$RP_1 = \tfrac{1}{2} \sum_{m=0}^{\infty} \sum_{n=0}^{\infty} \int_{-\infty}^{\infty} A_n (s\theta)^n H_{m+n}^{(2)}(s\theta) \cos (m\varphi + \gamma_m) U_1 \, s \, ds. \tag{2.37}$$

This form is adaptable to evaluation by residues or by stationary phase, depending on whether a normal mode representation, or a representation in terms of rays is desired.

The function U_1 is to be fixed by the boundary conditions. These require that the tangential electric and magnetic fields be continuous at $R = a$ and $R = h$. For this purpose both the electric and magnetic components of $[\Pi]$ will be required.

9

Hence we now consider the magnetic component Π_m in (2.1), and write

$$\Pi_m = k^2 \underset{\sim}{R} P_2.$$ (2.38)

Then P_2 satisfies the homogeneous equation

$$\nabla^2 P_2 + k^2 P_2 = 0.$$ (2.39)

The corresponding fields then are derivable from the equations

$$E_m = \text{curl}\,(\underset{\sim}{R} P_2),$$ (2.40)

$$H_m = \frac{i}{\omega \mu}\left[k^2 \underset{\sim}{R} P_2 + \text{grad}\,\frac{\partial}{\partial R}(R P_2)\right].$$ (2.41)

Solutions of (2.9) and (2.39) may be written in a form similar to (2.36) as

follows:

$$R P_2 = \sum_{m=0}^{\infty}\sum_{n=0}^{\infty}\int_{-\infty}^{\infty} \mathcal{A}\, A_n\,(s\theta)^n\, H^{(2)}_{m+n}\,(s\theta)\,\cos(m\varphi+\gamma_m)\,U_2\, s\, ds,$$ (2.42)

$$R P_3 = \sum_{m=0}^{\infty}\sum_{n=0}^{\infty}\int_{-\infty}^{\infty} \mathcal{E}\, A_n\,(s\theta)^n\, H^{(2)}_{m+n}\,(s\theta)\,\cos(m\varphi+\gamma_m)\,U_3\, s\, ds.$$ (2.43)

The constants $\mathcal{A}$ and $\mathcal{E}$ are to be determined by the boundary conditions at $R = a$

and $R = h$.

Corresponding to the physical picture of reflection at the boundaries, we

expect a mixture of upgoing and downgoing waves in the region $a<R<h$. We then

pick the two independent solutions of (2.12) to correspond to upgoing and downgoing

waves, and denote these by $U_1^{(2)}$ and $U_1^{(1)}$, respectively. A similar choice is made

for U_2 and U_3. The total field in the various regions then can be derived from a

radial P function which has the matrix form

$$\underset{\sim}{R}[P] = \underset{\sim}{R}\begin{bmatrix} P_1 + P_3 \\ P_2 \end{bmatrix},$$ (2.44)

in which

$$R P_n = T_n U_n V_n, \qquad n = 1,2,3.$$

The boundary conditions, being independent of θ and φ, lead directly to the

statements

$$T_1 = T_2 = T_3,$$

$$V_1 = V_2 = V_3.$$

Now we put

$$
\left.\begin{array}{l}
U_1 = U_1{}^{(1)} + U_1{}^{(2)}, \\
U_2 = U_2{}^{(1)} + U_2{}^{(2)}, \\
U_3 = U_3{}^{(1)} + U_3{}^{(2)},
\end{array}\right\} \tag{2.45}
$$

and introduce the reflection coefficient at the ground

$$
[\rho_g] = \begin{bmatrix} \rho_1 \\ \rho_2 \end{bmatrix} \tag{2.46}
$$

where ρ_1 and ρ_2 are the reflection coefficients for vertical and horizontal polarization, respectively. Then

$$
\begin{aligned}
U_1^{(2)}(a) &= \rho_1 U_1^{(1)}(a), \\
U_2^{(2)}(a) &= \rho_2 U_2^{(1)}(a), \\
U_3^{(2)}(a) &= \rho_1 U_3^{(1)}(a).
\end{aligned} \tag{2.47}
$$

At the ionosphere the reflection coefficient is a tensor

$$
[\rho_i] = \begin{bmatrix} \rho_{11} & \rho_{12} \\ \rho_{21} & \rho_{22} \end{bmatrix}, \tag{2.48}
$$

so that

$$
U_3^{(1)}(h) = \rho_{11}\left[U_1^{(2)}(h) + U_3^{(2)}(h)\right] + \rho_{12} U_2^{(2)}(h),
$$

$$
U_2^{(1)}(h) = \rho_{21}\left[U_1^{(2)}(h) + U_3^{(2)}(h)\right] + \rho_{22} U_2^{(2)}(h).
$$

Finally, at $R = b$ we have the discontinuity condition for the first derivative of U_1 in terms of the dipole moment [2]

$$
\frac{dU_1}{dR}\bigg|_{R=b-\epsilon}^{R=b+\epsilon} = \frac{i\omega\mu I\ell}{2\pi k b^2} \equiv K,
$$

while U_1 itself is continuous at $R = b$.

The radial functions U_2, U_3 satisfy the same type of differential equation as U_1, i.e. (2.12). If we denote the two independent solutions of this equation by $u^{(1)}$ and $u^{(2)}$, respectively, where $u^{(1)}$ represents a downgoing wave and $u^{(2)}$ an upgoing wave, then we may write in the various height regions

$$
U_1 = B_2\, u^{(2)}, \qquad\qquad b < R < h, \tag{2.49a}
$$

$$
U_1 = B_1\, u^{(1)} + B_2\, u^{(2)}, \qquad a < R < b, \tag{2.49b}
$$

$$
U_2 = A_1\, u^{(1)} + A_2\, u^{(2)}, \qquad a < R < h, \tag{2.49c}
$$

11

$$U_3 = \xi_1 u^{(1)} + \xi_2 u^{(2)}, \qquad a < R < h. \qquad (2.49d)$$

The boundary conditions then yield

$$\vartheta_2/\vartheta_1 = \rho_2 u^{(1)}(a)/u^{(2)}(a), \qquad (2.50a)$$

$$\mathcal{B}_2/\mathcal{E}_1 = \rho_1 u^{(1)}(a)/u^{(2)}(a), \qquad (2.50b)$$

$$\xi_2/\xi_1 = \rho_1 u^{(1)}(a)/u^{(2)}(a), \qquad (2.50c)$$

$$\vartheta_1 u^{(1)}(h) = [\rho_{21}(\vartheta_2 + \xi_2) + \rho_{22}\vartheta_2] u^{(2)}(h) \qquad (2.50d)$$

$$\xi_1 u^{(1)}(h) = [\rho_{11}(\vartheta_2 + \xi_2) + \rho_{12}\vartheta_2] u^{(2)}(h) \qquad (2.50e)$$

$$\vartheta_2 u^{(2)'}(b) = \xi_1 u^{(1)'}(b) + \xi_2 u^{(2)'}(b) + K, \qquad (2.50f)$$

$$\vartheta_2 u^{(2)}(b) = \xi_1 u^{(1)}(b) + \xi_2 u^{(2)}(b). \qquad (2.50g)$$

The seven equations (2.50a-g) are sufficient to determine the seven constants

ϑ_2, ξ_1, ξ_2, ϑ_1, ϑ_2, ξ_1, ξ_2. They are given by

$$\xi_1 = K/[(y_b - y_b') u^{(2)'}(b)] = \tfrac{1}{2}i K u^{(2)}(b), \qquad (2.51a)$$

$$\mathcal{F}_2 = \rho_1 y_a \xi_1, \qquad (2.51b)$$

$$\vartheta_2 = (\rho_1 y_a + y_b) \xi_1, \qquad (2.51c)$$

$$\vartheta_1 = M \xi_1 \qquad (2.51d)$$

$$\vartheta_2 = \rho_2 y_a \vartheta_1 = \rho_2 y_a M \xi_1 \qquad (2.51e)$$

$$\xi_1 = \frac{\rho_{11} - \rho_2 y_a \Delta}{\rho_{21} y_h} M \xi_1, \qquad (2.51f)$$

$$\xi_2 = \rho_1 y_a \xi_1 = (\rho_{11} - \rho_2 y_a \Delta)\frac{\rho_1 y_a}{\rho_{21} y_h} M \xi_1, \qquad (2.51g)$$

where

$$y_a = \frac{u^{(1)}(a)}{u^{(2)}(a)}, \qquad (2.52a)$$

$$y_b = \frac{u^{(1)}(b)}{u^{(2)}(b)}, \qquad (2.52b)$$

$$y_h = \frac{u^{(1)}(h)}{u^{(2)}(h)}, \qquad (2.52c)$$

$$y_b' = \frac{u^{(1)'}(b)}{u^{(2)'}(b)}, \qquad (2.52d)$$

$$M = \frac{\rho_{21} y_h (\rho_1 y_a + y_b)}{(\rho_{11} - \rho_2 y_a \Delta)(\rho_{22} - \rho_1 y_a \Delta) - \rho_{12}\rho_{21} y_h^2}$$

$$\Delta = \rho_{11}\rho_{22} - \rho_{12}\rho_{21}$$

primes denoting R-derivatives evaluated at the argument.

We now evaluate the form of the radial functions $u^{(1)}$ and $u^{(2)}$. These are solutions of

$$u'' + \left(k^2 - \frac{s^2}{R^2}\right)u = 0. \tag{2.53}$$

The solutions of this equation corresponding to downward and upward waves are the normalized spherical Hankel functions [5]

$$u^{(1)} = h_p^{(1)}(kR) = \left(\frac{\pi k R}{2}\right)^{1/2} H_p^{(1)}(kR), \tag{2.54}$$

$$u^{(2)} = h_p^{(2)}(kR) = \left(\frac{\pi k R}{2}\right)^{1/2} H_p^{(2)}(kR), \tag{2.55}$$

respectively, where

$$p = \left(s^2 + \tfrac{1}{4}\right)^{1/2}. \tag{2.56}$$

With these functions inserted in (2.49), the expressions (2.37), (2.42), (2.43) give the values for RP_s in the space $a \leq R \leq h$, from which the fields may be evaluated by (2.4), (2.5), (2.40), and (2.41).

2.4 Evaluation of the Integral Representation

Two different methods are available for evaluating the integral expressions for RP. By the method of stationary phase, the result may be expressed as a sum of rays reflected alternately a number of times from the ionosphere and the ground. By the method of residues, on the other hand, the result is obtained as a sum of normal modes, or waveguide-type waves. We shall investigate the latter type of solution in order to bring out the fact that the approximations usually made actually change the physical problem from that of a homogeneous atmosphere to that of a slightly inhomogeneous atmosphere.

Since the coefficients in the integrand $(\mathscr{B}_2 - \mathscr{E}_2)$ involve the y-functions defined above, which are ratios that are functions of s, the integrand has poles at zeros of the denominator in these ratios. Consequently, if we deform the integrand from the original contour along the real s-axis into the appropriate

half of the complex plane, the integral may be evaluated in terms of the
singularities of the integrand in that half-plane. In addition to the poles
just mentioned, there is also a branch point where the order of the spherical
Hankel functions, p, is zero. This can be seen from (2.56). This has branch
points at

$$s = \pm \tfrac{1}{2}i.$$

The integrand vanishes at infinite values of s in the lower half-plane.
Consequently the integration path is deformed into the contour shown in Fig. 2.
The integral then is the negative sum of the residues at the poles in the lower
half-plane, plus an integral around a branch cut along the negative imaginary
axis from -i/2. Friedman [2] has discussed the importance of the branch-cut
integral and has shown that it is negligible in practical cases. Wait [3], on
the other hand, attempts to avoid the branch-cut integral by making a double tra-
verse in the lower half-plane, but his procedure, in effect, is equivalent to
neglecting this integral. This integral represents the effect of the currents which
penetrate into the ground, and thus is essentially a part of the ground-wave field.
In the case of a perfectly-conducting ground the integral vanishes altogether.

The matrix $\underline{R}[P]$ in (2.44) has an integral representation which can be assem-
bled from (2.37), (2.42) and (2.43) by using the U-functions given in (2.49). Poles
of the integrand are those of the functions $\rho_{21}\psi_h$ and M. The principal poles of in-
terest in determining the normal modes are those of M. The investigation of these
poles is a separate problem in its own right which we shall not go into here. The
poles of $\rho_{21}\psi_h$, since ρ_{21} ultimately can be expressed in terms of y-functions and the
properties of the reflecting medium, can be expressed in terms of the two limiting
cases $\rho_{21} = -\psi_h$ and $\rho_{21} = -\psi_h'$, similar to the way in which Bremmer [6] treated the tropo-
spheric case. These can be determined from the zeros of $u^{(2)}(h)$ and $u^{(2)'}(h)$, respec-
tively. Thus we consider the method used for the determination of these zeros.

14
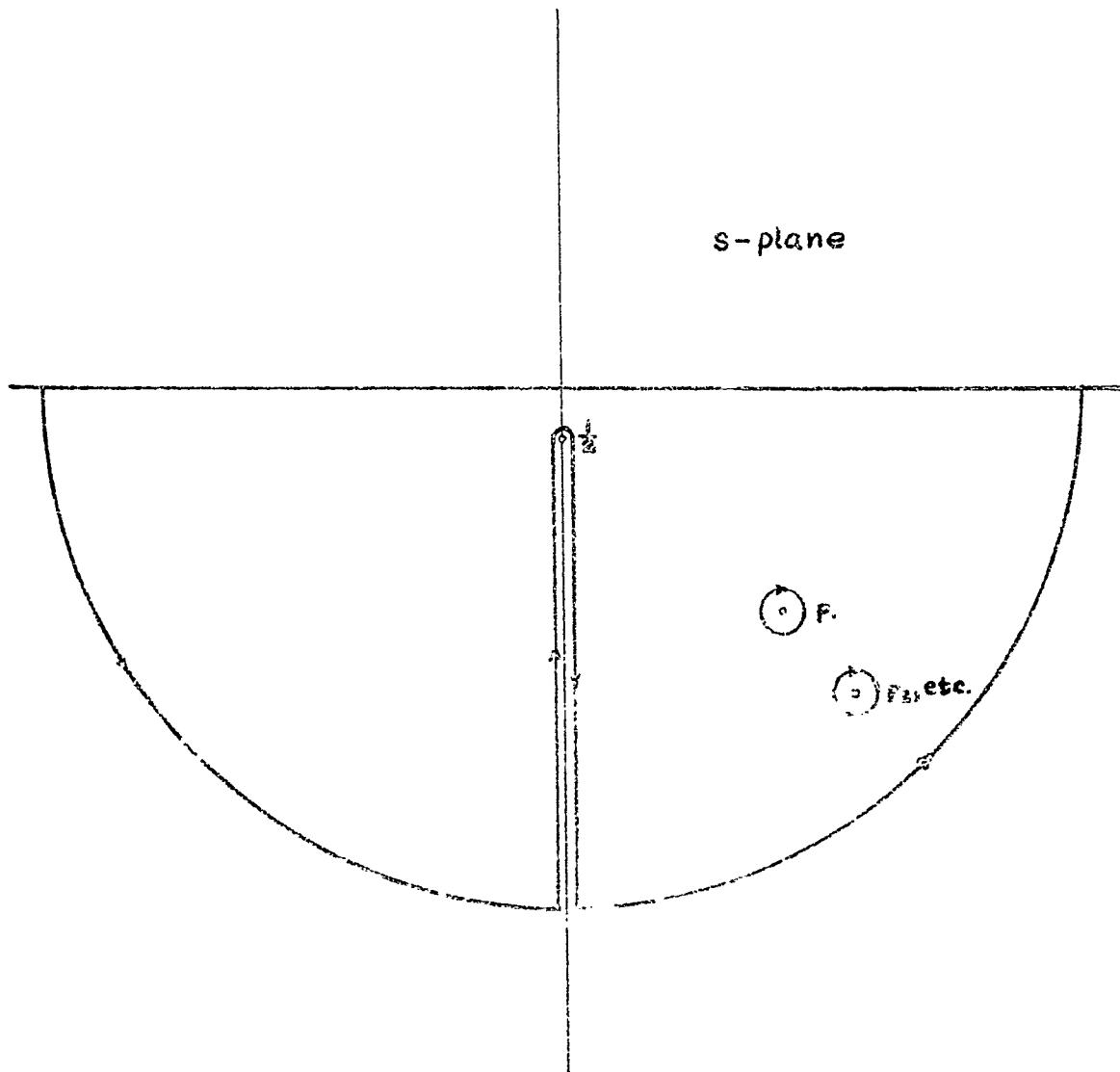
s-plane

Fig. 2 — Integration Contour in s-plane

2.5 The Complex Zeros of $u^{(2)}(z)$

The zeros of $u^{(2)}$ and $u^{(2)'}$ are the same as those of $H_p^{(2)}$ and $H_p^{(2)'}$. These are found by the Debye method of steepest descent, and are usually expressed in terms of Airy functions, or Hankel functions of order one-third. The procedure is to write

$$H_p^{(2)}(z) = \frac{1}{\pi}\int_{W_2} e^{i[z\cos w + p(w-\pi/2)]}\,dw = \frac{1}{\pi}\int_{W_2} e^{F(w)}\,dw, \tag{2.57}$$

expand the exponent $F(w)$ in a Taylor's series about the point where $F''(w) = 0$, and draw the contour W_2 so as to pass through the two points (stationary points) at which $F'(w) = 0$. By truncating the Taylor's series expansion of $F(w)$ at the third derivative term, we obtain

$$F(w) \approx F(w_0) + (w-w_0)F'(w_0) + \frac{(w-w_0)^3}{3!}F'''(w_0).$$

Since

$$F''(w_0) = -iz\cos w_0 = 0,$$

we have

$$w_0 = \pi/2,$$

and

$$F(w_0) = 0,$$
$$F'(w_0) = -i(z-p),$$
$$F'''(w_0) = iz.$$

Consequently, upon putting $w - w_0 = u$, (2.57) becomes

$$H_p^{(2)}(z) \approx \frac{1}{\pi}\int_{U_2} e^{-i(z-p)u + izu^3/6}\,du,$$

where the contour U_2 is merely W_2 shifted to the right by $\pi/2$. A simple change of variables

$$\left.\begin{array}{l} t = (iz/2)^{1/3}u \\[2mm] \varsigma = 2^{1/3}z^{-1/3}(z-p)\,e^{-i2\pi/3} \end{array}\right\} \tag{2.58}$$

16

results in

$$H_p^{(2)}(z) \approx \frac{2^{1/3}}{\pi} z^{-1/3} e^{-i\pi/6} \int_{L_2} e^{\varsigma t + t^3/3} dt, \qquad (2.59)$$

where the contour L_2 in the t-plane is shown in Fig. 3. The integral in (2.59) may be expressed in terms of the Airy Functions, or Modified Hankel Functions of order one-third [7]. Using the notation for the latter,

$$h_2(\varsigma) = \frac{(12)^{1/6}}{\pi} e^{i2\pi/3} \int_{L_2} e^{\varsigma t + t^3/3} dt,$$

we obtain

$$H_p^{(2)}(z) \approx 3^{-1/6} z^{-1/3} e^{-i5\pi/6} h_2(\varsigma). \qquad (2.60)$$
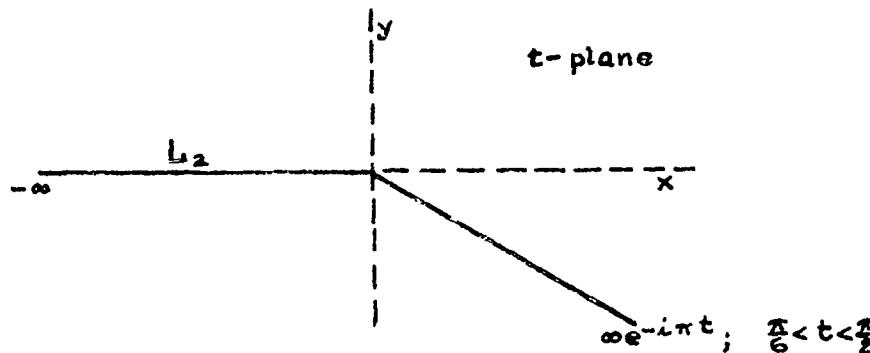
Fig. 3 — Contour for Modified Hankel Functions

Then from (2.55)

$$\mathcal{U}^{(2)} = h_p^{(2)}(z) = \left(\frac{\pi z}{2}\right)^{1/2} H_p^{(2)}(z),$$
$$\approx (24)^{-1/6} \pi^{1/2} z^{1/6} e^{-i5\pi/6} h_2(\varsigma). \qquad (2.61)$$

Consequently the zeros of $h_2(\varsigma)$ (tabulated in [7]) give, in first approximation, the zeros of $H_p^{(2)}(z)$ and of $h_p^{(2)}(z)$.

It was pointed out in [1] that the approximation (2.61) is equivalent to a change in the physical problem. This is immediately evident from the fact that $h_p^{(2)}(z)$ is a solution of (2.12), while $h_2(\varsigma)$ is a solution of Stokes' equation

$$\frac{d^2 h_2}{d\varsigma^2} + \varsigma h_2 = 0. \qquad (2.62)$$

The physical problem corresponding to (2.61) may be found as follows:

We first separate (2.9) by writing P_1 in the form

$$P_1 = T(\theta)\, U_o(R)\, V(\varphi),$$

whereby the radial equation becomes

$$\frac{d^2 U_o}{dR^2} + \frac{2}{R}\frac{dU_o}{dR} + \left(k^2 - \frac{s^2}{R^2}\right) U_o = 0.$$

Now by introducing the transformation

$$\eta = a\,\log(R/a),$$

the radial equation becomes

$$\frac{d^2 U_o}{d\eta^2} + \frac{1}{a}\frac{dU_o}{d\eta} + \left(k^2 e^{2\eta/a} - \frac{s^2}{a^2}\right) U_o = 0.$$

Next, putting

$$U_o = u_o\, e^{-\frac{\eta}{2a}} = \left(\frac{a}{R}\right)^{1/2} u_o,$$

we obtain

$$\frac{d^2 u_o}{d\eta^2} + \left(k^2 e^{2\eta/a} - \sigma^2\right) u_o = 0, \tag{2.63}$$

where

$$\sigma^2 = \frac{1}{a^2}\left(s^2 + 1/4\right) = p^2/a^2.$$

To reduce this to Stokes' equation, we must have

$$k^2 e^{2\eta/a} = k_o^2\left(1 + q\eta\right), \tag{2.64}$$

where k_o and q are constants. It is evident from (2.63) that $q = 2/a$ in order to satisfy the equation for small η. In this case, if we put

$$S^2 = \sigma^2/k_o^2,$$

$$\zeta = (k_o/q)^{2/3}\left(1 - S^2 + q\eta\right),$$

we obtain, finally, Stokes' equation

$$\frac{d^2 u_o}{d\zeta^2} + \zeta u_o = 0,$$

a solution of which is

$$u_o = h_2(\zeta).$$

In order to arrive at this solution, however, k must be a function of η which

satisfies (2.64). In terms of the variable R, this requires that k have the form

$$\frac{k(R)}{k_o} = n(R) = \frac{(1 + 4a \log R/a)^{1/2}}{R/a} = \frac{(1 + 2 \log R/a)^{1/2}}{R/a}. \tag{2.65}$$

If we put

$$R = a + H = a\left(1 + \frac{H}{a}\right),$$

then we have

$$n(R) = \frac{\left[1 + 2 \log\left(1 + \frac{H}{a}\right)\right]^{1/2}}{1 + \frac{H}{a}} \approx 1 - \left(\frac{H}{a}\right)^2 + \cdots.$$

Thus the refractive index (2.65), corresponding to Stokes' equation, decreases monotonically with increasing height H above the ground level a, whereas the original problem dealt with a constant refractive index.

To obtain a higher order approximation for the zeros of $H_p^{(2)}(z)$, one may follow a procedure due to Olver [8] and Chester, Friedman, and Ursell [9], whereby a change of variable is introduced so that $F(w)$ in (2.57) becomes precisely the exponent in the integral of (2.59):

$$F(w) = \zeta t + t^3/3,$$
$$\frac{dw}{dt} = \frac{\zeta + t^2}{F'(w)} = \frac{\zeta + t^2}{-i(z \sin w - p)}.$$

Then (2.57) becomes

$$H_p^{(2)}(z) = \frac{1}{\pi} \int_{L_2} e^{\zeta t + t^3/3} \frac{dw}{dt} dt. \tag{2.66}$$

By expanding $\frac{dw}{dt}$ in a double series of the form

$$\frac{dw}{dt} = \sum_{m=0}^{\infty} p_m (t^2 + \zeta)^m + \sum_{m=0}^{\infty} q_m t (t^2 + \zeta)^m, \tag{2.67}$$

and integrating (2.66) termwise, an asymptotic expansion is obtained in terms of $h_2(\zeta)$ and $h_2'(\zeta)$

$$H_p^{(2)}(z) \sim 3^{-1/6} z^{-1/3} e^{-i 5\pi/6} \left\{ h_2(\zeta) \sum_{m=0}^{\infty} A_m + h_2'(\zeta) \sum_{m=0}^{\infty} B_m \right\}, \tag{2.68}$$

in which the coefficients A_m and B_m involve, in general, inverse fractional powers of z, except that $A_0 = 1$.

The above procedure is asymptotic because the series expansion (2.67) has a radius of convergence which is limited by the next zero of $F'(w)$, which occurs at

19

$w = \pi - \sin^{-1}(p/z)$, while the interval of integration extends to infinity.

An alternative evaluation of (2.57) which is not of asymptotic character may be developed, however. This does not appear to have been reported previously. We write

$$F(w) = \varsigma t + t^3/3 + \mathcal{R},$$

where ς and t are given by (2.58), and

$$\mathcal{R} = \sum_{n=4}^{\infty} (iz/2)^{-n/3} \frac{F^{(n)}(w_0)}{n!} t^n,$$
$$= 2 \sum_{n=2}^{\infty} (-)^{n+1} (iz/2)^{-(2n-2)/3} \frac{t^{2n+1}}{(2n+1)!} = \sum_{n=2}^{\infty} a_n t^{2n+1}.$$

Next we write

$$e^{F(w)} = e^{\varsigma t + t^3/3} \cdot e^{\mathcal{R}}$$

and expand $e^{\mathcal{R}}$ in the absolutely convergent series

$$e^{\mathcal{R}} = \sum_{m=0}^{\infty} \frac{\mathcal{R}^m}{m!} = \sum_{m=0}^{\infty} \frac{1}{m!} \left[\sum_{n=2}^{\infty} a_n t^{2n+1} \right]^m$$
$$\equiv P(t) = 1 + \sum_{m=5}^{\infty} b_m t^m.$$

The integral (2.57) then becomes

$$H_p^{(2)}(z) = \frac{1}{\pi} (iz/2)^{-1/3} \int_{L_2} P(t) e^{\varsigma t + t^3/3} dt.$$

Termwise integration then yields an expression of identically the same form as (2.68),

$$H_p^{(2)}(z) = 3^{-1/6} z^{-1/3} e^{-i5\pi/6} \left\{ \alpha(\varsigma) h_2(\varsigma) + \beta(\varsigma) h_2'(\varsigma) \right\}, \tag{2.69}$$

where

$$\alpha(\varsigma) = 1 + \sum_{m=5}^{\infty} b_m A_m(\varsigma),$$
$$\beta(\varsigma) = \sum_{m=5}^{\infty} b_m B_m(\varsigma),$$

$A_m(\varsigma)$ and $B_m(\varsigma)$ being polynomials in ς of degree $m/2$ or less.

Then

$$h_p^{(2)}(z) = \left(\frac{\pi z}{2} \right)^{1/2} H_p^{(2)}(z),$$
$$= (24)^{-1/6} \pi^{1/2} z^{1/6} e^{-i5\pi/6} \left\{ \alpha(\varsigma) h_2(\varsigma) + \beta(\varsigma) h_2'(\varsigma) \right\}. \tag{2.70}$$

It is evident from (2.69) that the zeros of $H_p^{(2)}(z)$, for given z, differ

20

slightly from the zeros of $h_2(\varsigma)$, where ς is related to z and p by (2.58). In order to find the values of p for which $H_p^{(2)}(z)$ is zero, we can proceed as follows:

Denote the zeros of $h_2(\varsigma)$ by ς_0, so that

$$h_2(\varsigma_0) = 0. \qquad (2.71)$$

From (2.69) we then find

$$H_p^{(2)}(z) = 3^{-1/6} z^{-1/3} e^{-i 5\pi/6} \beta(\varsigma_0) h_2'(\varsigma_0) = 0.$$

The value of p corresponding to ς_0 is near a zero of $H_p^{(2)}(z)$. We denote this zero by σ, i.e.,

$$H_\sigma^{(2)}(z) = 0,$$

and put

$$p = \sigma - q. \qquad (2.72)$$

σ, which as yet is unknown, corresponds to a value of ς which we denote by

$$\varsigma = \varsigma_0 + \varsigma_1. \qquad (2.73)$$

so that ς_1 is small compared to ς_0. Then by (2.69)

$$H_\sigma^{(2)}(z) = 0 = \alpha(\varsigma_0 + \varsigma_1) h_2(\varsigma_0 + \varsigma_1) + \beta(\varsigma_0 + \varsigma_1) h_2'(\varsigma_0 + \varsigma_1).$$

We now expand α, β, h_2, and h_2' in Taylor's series about ς_0, and make use of (2.71):

$$\alpha(\varsigma) = \alpha_0 + \varsigma_1 \alpha_0' + \frac{\varsigma_1^2}{2!} \alpha_0'' + \cdots,$$

$$\beta(\varsigma) = \beta_0 + \varsigma_1 \beta_0' + \frac{\varsigma_1^2}{2!} \beta_0'' + \cdots,$$

$$h_2(\varsigma) = h_2'(\varsigma_0) \cdot \left\{ \varsigma_1 - \varsigma_0 \frac{\varsigma_1^3}{3!} - 2 \frac{\varsigma_1^4}{4!} + \varsigma_0^2 \frac{\varsigma_1^5}{5!} + \cdots \right\}$$

$$\equiv \eta_1 h_2'(\varsigma_0),$$

$$h_2'(\varsigma) = h_2'(\varsigma_0) \cdot \left\{ 1 - \varsigma_0 \frac{\varsigma_1^2}{2!} - 2 \frac{\varsigma_1^3}{3!} + \varsigma_0^2 \frac{\varsigma_1^4}{4!} + \cdots \right\}$$

$$\equiv \eta_2 h_2'(\varsigma_0).$$

Consequently we obtain

$$\eta_1 \alpha(\varsigma) + \eta_2 \beta(\varsigma) = 0.$$

This is a series in ς_1, whose coefficients are known. The value of ς_1 then may be obtained by successive approximations. Then from (2.58), (2.72) and (2.73),

we obtain

$$q = 2^{-1/3} z^{1/3} e^{i\,2\pi/3} \varsigma_1 .$$

(2.74)

The required zeros of $H_p^{(2)}(z)$ then are

$$p = \sigma - q .$$

These likewise are the zeros of the modified spherical Hankel function $h_p^{(2)}(z)$ given by (2.70).

The detailed results obtainable by this procedure will be reserved for a later investigation.

3. NON-SPHERICALLY STRATIFIED IONOSPHERE

In the treatment in Sec. 2, the earth-ionosphere region was assumed to be spherically symmetrical (so-called "horizontally-stratified" medium). This situation is not strictly true, in general, so that the above type of analysis is an idealization which should be considered as only a first approximation to the true state of affairs. For example, there are situations of practical interest where the reflecting layers are tilted with respect to the horizontal.

In order to introduce a form of non-spherical stratification which may be applicable to such situations, we consider the case of a spheroidal geometry, where the earth and ionosphere are coordinate surfaces of a family of spheroids, either oblate or prolate in form. We give below the extension of the exact earth-flattening procedure to this non-spherical geometry.

3.1 Formulation of the Problem

The reduced wave equation

$$\nabla^2 P + k^2 P = 0$$

may be separated in spheroidal coordinates into radial and angular differential equations as in the spherical case. For the oblate spheroid, these are

$$\frac{d^2U}{d\xi^2} + \tanh\xi \frac{dU}{d\xi} + \left(k^2f^2\cosh^2\xi - s^2 + \frac{m^2}{\cosh^2\xi}\right)U = 0,$$

$$\frac{d^2T}{d\theta^2} + \cot\theta \frac{dT}{d\theta} - \left(k^2f^2\sin^2\theta - s^2 + \frac{m^2}{\sin^2\theta}\right)T = 0, \qquad (3.1)$$

$$\frac{d^2V}{d\varphi^2} + m^2V = 0,$$

where f is the semi-focal distance, and a typical space point has the rectangular coordinates

$$x = f\cosh\xi \cos\theta \cos\varphi,$$

$$y = f\cosh\xi \cos\theta \sin\varphi,$$

$$z = f\sinh\xi \sin\theta.$$

The corresponding equations of the prolate spheroid are

$$\frac{d^2U}{d\xi^2} + \coth\xi \frac{dU}{d\xi} + \left(k^2f^2\sinh^2\xi - s^2 - \frac{m^2}{\sinh^2\xi}\right)U = 0,$$

$$\frac{d^2T}{d\theta^2} + \cot\theta \frac{dT}{d\theta} + \left(k^2f^2\sin^2\theta + s^2 - \frac{m^2}{\sin^2\theta}\right)T = 0, \qquad (3.2)$$

$$\frac{d^2V}{d\varphi^2} + m^2V = 0,$$

for which a typical space point has the rectangular coordinates

$$x = f\sinh\xi \sin\theta \cos\varphi,$$

$$y = f\sinh\xi \sin\theta \sin\varphi,$$

$$z = f\cosh\xi \cos\theta.$$

We shall treat the oblate case in detail, since a comparison of the corresponding equations of (3.1) and (3.2) shows that a change from (3.1) to (3.2) can be effected by simple transformations.

3.2 The Angular Function T

We consider first the angular function T. Introducing the new independent variable $x = s\theta$, as in Sec. 2.2, the second equation of (3.1) becomes

$$\frac{d^2T}{dx^2} + \frac{1}{s}\cot\left(\frac{x}{s}\right)\frac{dT}{dx} + \left[1 - \frac{k^2f^2}{s^2}\sin^2\left(\frac{x}{s}\right) - \frac{m^2}{s^2}\csc^2\left(\frac{x}{s}\right)\right]T = 0. \qquad (3.3)$$

This may be written as

$$L(T) \equiv T'' + \frac{1}{x}T' + \left(1 - \frac{m^2}{x^2}\right)T = \left[\frac{1}{x} - \frac{1}{s}\cot\left(\frac{x}{s}\right)\right]T' - \left\{m^2\left[\frac{1}{x^2} - \frac{1}{s^2}\csc^2\left(\frac{x}{s}\right)\right] + \frac{k^2f^2}{s^2}\sin^2\left(\frac{x}{s}\right)\right\}T$$

$$= \sum_{\mu=1}^{\infty} \left\{a_\mu\left[\frac{1}{x}T' - (2\mu-1)\frac{m^2}{x^2}T\right] + b_\mu k^2 T\right\}\left(\frac{x}{s}\right)^{2\mu} \qquad (3.4)$$

23

where

$$\kappa = kf, \tag{3.5}$$

$$a_\mu = 2^{2\mu} B_\mu /(2\mu)! \tag{3.6}$$

$$b_\mu = (-)^{\mu+1} 2^{2\mu-1}/(2\mu)! \tag{3.7}$$

(3.4) is similar in form to (2.21), and differs from it only in the presence on the right-hand side of the additional term $b_\mu \kappa^2 (x/s)^{2\mu} T$. This term has the same power of x as the $(\mu+1)$-th term immediately preceding it in (3.4). Consequently we can immediately write the solution of (3.4) as

$$T = \sum_{n=0}^{\infty} a_n C_{m,n}, \tag{3.8}$$

where the coefficients a_n are given by the recursion formula

$$a_{n+1} = A_{n+1} + \frac{1}{2(n+1)} \sum_{p=0}^{n-1} \sum_{\mu \geq \frac{n-p-1}{2}}^{n-p-1} c_{p,\mu+1,n-p-\mu-1} b_{\mu+1} \kappa^2 A_p s^{-2(\mu+1)}$$

$$= \frac{1}{2(n+1)} \left\{ \sum_{p=0}^{n} \sum_{\mu \geq \frac{n-p}{2}}^{n-p} D c_{p,\mu,n-p-\mu} a_{\mu+1} \right.$$

$$\left. + \sum_{p=0}^{n-1} \sum_{\mu \geq \frac{n-p-1}{2}}^{n-p-1} \left[c_{p,\mu+1,n-p-\mu-1} b_\mu \kappa^2 - c_{p+1,\mu,n-p-\mu-1} a_{\mu+1} \right] \right\} A_p s^{-2(\mu+1)}. \tag{3.9}$$

Therefore the form of solution given in (2.35) is directly applicable to (3.3), which thus has the solution

$$T = \sum_{n=0}^{\infty} a_n (s\theta)^n J_{m+n} (s\theta). \tag{3.10}$$

3.3 The Radial Function U

We now consider the radial function U, which satisfies the first equation of (3.1). Our aim will be to obtain a solution of this equation similar to that found in Sec. 2.3. Then the fields will be obtainable in terms of an integral representation of the form given in (2.36). We shall be interested in the normal mode solution, which is obtainable from the residues of the integral representation. These residues, as in the spherical case, ultimately may be based on the zeros of the function U which represents an upgoing wave, and its first derivative. Consequently, we shall seek solutions of the radial equation similar

to those given in (2.54) and (2.55) for the spherical case, and then will investigate their complex zeros as a function of order.

The radial equation in question is

$$\frac{d^2 U}{d\xi^2} + \tanh\xi \frac{dU}{d\xi} + \left(k^2 f^2 \cosh^2\xi - s^2 + \frac{m^2}{\cosh^2\xi}\right)U = 0. \tag{3.11}$$

We seek to cast this into a form which resembles the spherical equation.

We first note that the transition to the spherical case is effected by allowing $f \cosh\xi \to R$ as $f \to 0$. Hence we are led to introduce the change of independent variable

$$f \cosh\xi = R, \tag{3.12}$$

and the new dependent variable

$$u = RU.$$

Then (3.11) becomes

$$\frac{d^2 u}{dR^2} + \frac{f^2}{R(R^2 - f^2)}\frac{du}{dR} + \frac{1}{R^2 f^2}\left[k^2 R^2 - s^2 + \frac{(m^2 - 1)f^2}{R^2}\right]u = 0. \tag{3.13}$$

Next, we put

$$z = kR,$$
$$a = kf, \tag{3.14}$$

whereupon (3.13) becomes

$$u'' + \frac{a^2}{z(z^2 - a^2)}u' + \frac{z^2}{z^2 - a^2}\left(1 - \frac{s^2}{z^2} + \frac{(m^2 - 1)a^2}{z^4}\right)u = 0, \tag{3.15}$$

primes denoting derivatives with respect to z.

To eliminate the first-derivative term, we put

$$u = \left(\frac{z^2}{z^2 - a^2}\right)^{1/4} v; \tag{3.16}$$

(3.16) then is replaced by

$$v'' + \left[\frac{z^2 - s^2}{z^2 - a^2} + \frac{(m^2 - 1)a^2}{z^2(z^2 - a^2)} + \frac{3}{4}\frac{(2z^2 - a^2)a^2}{z^2(z^2 - a^2)^2}\right]v = 0. \tag{3.17}$$

We now rearrange (3.17) in the form

$$L(v) \equiv v'' + \left(1 - \frac{s^2}{z^2}\right)v = -\frac{a^2}{z^2 - a^2}\left[1 + \frac{m^2 - s^2 + 1/2}{z^2} + \frac{3/4\, a^2}{z^2(z^2 - a^2)}\right]v$$

$$= -\sum_{\mu=0}^{\infty}\left(\frac{a}{z}\right)^{2\mu+2}\left[1 + \frac{m^2 - s^2 + 1/2}{a^2}\left(\frac{a}{z}\right)^2 + \frac{3}{4}(\mu+1)\left(\frac{a}{z}\right)^4\right]v,$$

25

or

$$L(v) = \sum_{\mu=0}^{\infty} \gamma_\mu \left(\frac{a}{z}\right)^{2\mu+2} v, \tag{3.18}$$

where

$$\gamma_0 = -1$$

$$\gamma_1 = -\left[1 + \frac{m^2 - 3^2 + \frac{1}{2}}{a^2}\right] = -\left[1 + \frac{m^2 - p^2 + \frac{3}{4}}{a^2}\right], \tag{3.19}$$

$$\gamma_\mu = -\left[1 + \frac{m^2 - p^2 + \frac{3}{4}}{a^2}\right] + \frac{3}{4}(\mu-1)\Big], \quad \mu \geq 2.$$

If the right-hand side of (3.18) were zero (i.e., a = 0), solutions of the equation would be the normalized spherical Hankel functions given by (2.54) and (2.55). Hence we seek a similar solution to (3.18). Solutions of the radial equation as a series of solutions of the spherical Bessel differential equation are available in the literature (see, for example, [10]), but we shall find it more convenient to deduce directly a special form which is suitable for the normal mode problem.

The form of (3.18) suggests a series solution in a/z. Such a solution may be formed in the form

$$v = \sum_{\nu=0}^{\infty} \left[A_\nu \left(\frac{a}{z}\right)^{2\nu} \mathcal{J}_p(z) + B_\nu \left(\frac{a}{z}\right)^{2\nu-1} \mathcal{J}_p'(z)\right], \tag{3.20}$$

where $\mathcal{J}_p$ is a solution of the normalized spherical Bessel equation $L(\mathcal{J}_p) = 0$ and $B_0 = 0$. Substituting (3.20) into (3.18), reducing by means of the differential equation for $\mathcal{J}_p$ to terms containing only $\mathcal{J}_p$ and $\mathcal{J}_p'$, and equating coefficients of like powers of $\mathcal{J}_p$ and $\mathcal{J}_p'$ on both sides of the equation, we obtain the two equations

$$-\frac{4\nu}{a}A_\nu + \left[1 + \frac{2\nu(2\nu-1)}{a^2}\right] B_\nu = \sum_{\lambda=0}^{\nu-1} B_\lambda \gamma_{\nu-\lambda}, \tag{3.21}$$

$$\left[1 + \frac{2\nu(2\nu+1)}{a^2}\right] A_\nu + \frac{2(2\nu+1)}{a} B_{\nu+1} - \frac{4\nu s^2}{a^3} B_\nu = \sum_{\lambda=0}^{\nu-1} A_\lambda \gamma_{\nu-\lambda}. \tag{3.22}$$

These are two simultaneous equations which comprise recurrence relations for the coefficients A_ν and B_ν in (3.20). If we choose $A_0 = 1$, then the first few coefficients are

$$B_1 = -\frac{a}{2}, \qquad\qquad A_1 = -\frac{1}{4} - \frac{a^2}{8},$$

$$B_2 = \frac{a^3}{48} - \frac{(m^2 + p^2 - 5/4)}{6a}, \qquad A_2 = \frac{a^4}{384} + \frac{3a^2}{32} + \frac{m^2 - 2p^2 + 7/4}{24} - \frac{m^2 + p^2 - 5/4}{4a^2}.$$

26

Thus combining (3.20) and (3.16), we have found a solution of (3.15) of the form

$$u(z) = \alpha(z)\jmath_p(z) + \mathcal{B}(z)\jmath_p'(z), \tag{3.23}$$

where

$$\alpha(z) = \left(\frac{z^2}{z^2-a^2}\right)^{1/4} \sum_{\nu=0}^{\infty} A_\nu \left(\frac{a}{z}\right)^{2\nu}, \tag{3.24}$$

$$\mathcal{B}(z) = \left(\frac{z^2}{z^2-a^2}\right)^{1/4} \sum_{\nu=1}^{\infty} B_\nu \left(\frac{a}{z}\right)^{2\nu-1}. \tag{3.25}$$

In order to conform to the type of integral representation given for the spherical case in Sec. 2, we choose the function $\jmath_p$ to be the normalized spherical Hankel function $h_p^{(1)}$ or $h_p^{(2)}$. Then in finding the normal mode solution for the spheroidal problem we are led to a determination of the zeros of the function

$$u_p^{(2)}(z) = \alpha(z) h_p^{(2)}(z) + \mathcal{B}(z) h_p^{(2)'}(z). \tag{3.26}$$

We can reduce this problem to one of exactly the same kind as solved in Sec. 2.5. From (2.70), we can replace $h_p^{(2)}(z)$ by a suitable sum of $h_2(\varsigma)$ and $h_2'(\varsigma)$ as follows:

$$h_p^{(2)}(z) = (24)^{-1/6} \pi^{1/2} z^{1/6} e^{-i5\pi/6} \left[\alpha(\varsigma) h_2(\varsigma) + \beta(\varsigma) h_2'(\varsigma)\right]. \tag{3.27}$$

From this,

$$h_p^{(2)'}(z) = (24)^{-1/6} \pi^{1/2} z^{1/6} e^{-i5\pi/6} \left\{\left[\frac{\alpha(\varsigma)}{6z} - \varsigma\beta(\varsigma)\right] h_2(\varsigma) + \left[\alpha(\varsigma) + \frac{\beta(\varsigma)}{6z}\right] h_2'(\varsigma)\right\}, \tag{3.28}$$

where use has been made of (2.62) to eliminate $h_2''(\varsigma)$.

Introducing (3.27) and (3.28) into (3.26), we obtain

$$u_p^{(2)}(z) = (24)^{-1/6} \pi^{1/2} z^{1/6} e^{-i5\pi/6} \left[\alpha_1(\varsigma) h_2(\varsigma) + \beta_1(\varsigma) h_2'(\varsigma)\right], \tag{3.29}$$

where

$$\alpha_1(\varsigma) = \alpha \alpha(\varsigma) + \mathcal{B}\left[\frac{\alpha(\varsigma)}{6z} - \varsigma\beta(\varsigma)\right] \tag{3.30}$$

$$\beta_1(\varsigma) = \alpha \beta(\varsigma) + \mathcal{B}\left[\alpha(\varsigma) + \frac{\beta(\varsigma)}{6z}\right] \tag{3.31}$$

(3.29) now is of the same form as (2.70). Consequently the procedure by which the zeros of (2.70) were found may be applied directly to (3.29), the only change required being the replacement of $\alpha(\varsigma)$ and $\beta(\varsigma)$ by $\alpha_1(\varsigma)$ and $\beta_1(\varsigma)$, respectively.

27

4. SUMMARY

In this report we have shown how the exact earth-flattening procedure, developed in [1] for an isotropic spherically-stratified atmosphere, may be extended to the case of a spherical earth and atmosphere enveloped by a sharply bounded ionosphere. The general solution of the problem is formulated as an integral representation, from which may be derived either a ray-optical series or a normal mode series. In the latter case, the normal modes involve the normalized spherical Hankel function and its derivative. An improved method of obtaining the zeros of these functions is derived which is not of asymptotic character.

In order to deal with problems of non-spherical stratification, a spheroidal geometry is investigated. The developments for the spheroidal case are pursued in a way similar to that for the spherical geometry, and carried out in detail for the oblate spheroid. Solutions for the angular function are found in the form of an infinite series of Bessel functions of the same type as found for the spherical case. The radial function is expressed as a sum of the solution of the normalized spherical Bessel equation and its derivative, the coefficients of these functions being infinite series in terms of powers of the ratio of semi-focal distance to radius. It is shown that the zeros of the radial function as a function of order, which are required in the normal mode solution, may be found by the same procedure that was developed for the spherical case.

REFERENCES

[1] B. Y.-C. Koo and M. Katzin, "An Exact Earth-Flattening Procedure in Propagation Around a Sphere", Jour. Res. NBS - D. Radio Propagation, Vol. 64D, No. 1, pp. 61-64, Jan.-Feb. 1960.

[2] B. Friedman, "Propagation in a Non-homogeneous Atmosphere", Comm. on Pure and App. Math., Vol. IV, No. 2/3, pp. 317-350, 1951.

[3] J. R. Wait, "Terrestrial Propagation of Very-Low-Frequency Radio Waves - A Theoretical Investigation", Jour. Res. NBS - D. Radio Propagation, Vol. 64D, No. 2, pp. 153-204, March-April 1960.

[4] J. C. Slater, "Microwave Transmission", pp. 197-199, McGraw-Hill Book Co., Inc., New York, 1942.

[5] S. A. Schelkunoff, "Advanced Antenna Theory", p. 8, John Wiley & Sons, Inc., New York, 1952.

[6] H. Bremmer, "Terrestrial Radio Waves", Elsevier Publishing Co., Inc., New York, 1949.

[7] The Staff of the Computation Laboratory, "Tables of the Modified Hankel Functions of Order One-Third and of Their Derivatives", Harvard Univ. Press, Cambridge, Mass., 1945.

[8] F. W. J. Olver, "The Asymptotic Expansion of Bessel Functions of Large Order", Phil. Trans. Roy. Soc., Series A, Vol. 247, pp. 328-367, Dec. 1954.

[9] C. Chester, B. Friedman and F. Ursell, "An Extension of the Method of Steepest Descents", Proc. Camb. Phil. Soc., Vol. 53, pp. 599-611, 1957.

[10] C. Flammer, "Spheroidal Wave Functions", Stanford Univ. Press, Stanford, Calif., 1957.

PART II

VLF ENHANCEMENTS AND HF FADEOUTS DURING

SUDDEN IONOSPHERIC DISTURBANCES

1. INTRODUCTION

One of the spectacular phenomena of the ionosphere is the sudden ionospheric disturbance (SID), which drastically affects high-frequency communication circuits. This phenomenon was first reported by Mögel [1]* and later investigated in detail by Dellinger [2]. Dellinger summarized the various phenomena associated with the SID and concluded that the disturbance must be caused by solar ultraviolet radiation. One of the associated phenomena occurs on very low frequencies, and it is this phenomenon that forms the subject matter of the present study.

In 1936, Bureau and Maire [3] reported that abrupt short-wave fade-outs (denoted by SWF hereafter) usually were accompanied by simultaneous sudden increases in the strength of atmospherics received on very low frequencies (vlf). They reported that atmospherics from all directions were reinforced simultaneously, that frequencies from 27 to 40 kc/s showed the sudden increase, but on 12 kc/s the effect was rarely observed. Later, Budden and Ratcliffe [4] reported that measurements at Cambridge of the phase of the abnormal (horizontally-polarized) component of the downcoming waves from GBR on 16 kc/s showed an anomaly at times of h-f fade-out. They concluded that an SID "has a marked effect at the level of reflection of the low-frequency waves (70 km), this effect being most evident as a decrease in reflection height of the waves". They did not observe "any clear indication of a change in reflected wave amplitude at the time of the phase anomalies" (SPA). Bureau [5] then pointed

---

*Numbers in brackets refer to the corresponding references in the Bibliography on p. 52.

30

out that his observations on the sudden enhancement of atmospherics (SEA) accompanying SID showed that such increases were not observed below about 17 kc/s.

An investigation was undertaken in 1938 to determine whether SID, which had been shown to produce SEA, also produced similar enhancement of v-l-f radio signals, and, if so, whether any quantitative correlation existed between the v-l-f and h-f effects of the SID. The experimental phase of the investigation was completed in 1940, and a preliminary report of the results was presented in 1947 [6], but has not been published.

The purpose of this report is to present the essential results obtained, and to discuss the implications of these results with respect to ionospheric layer structure and the modifications produced therein by the SID mechanism.

2. DESCRIPTION OF MEASUREMENTS

The measurements reported here were made at the Riverhead transcontinental receiving station of RCA Communications, Inc. After several months' observations of the signal from SAQ (17.2 kc/s), with negative results, the equipment was set up to record GLC (31.15 kc/s). Some of the subsequent SWF were accompanied by sudden signal enhancements (SSE) of GLC. Consequently, observations were continued, extending over the period 31 October 1938 to 25 June 1940.

For comparison of the v-l-f SSE with SWF, the signal received from GLH (13.53 Mc/s) was selected, since this signal traversed approximately the same path, and continuous recording of this signal was being carried out at Riverhead for other purposes. The great circle path length was about 5400 km. Both the GLC and the GLH equipments were calibrated at least once each day by means of standard signal generators.

3. RESULTS

Sample records of a simultaneous SWF and SSE are reproduced in Figs. 1

31

and 2, respectively. These records are rather typical of the data obtained, although the magnitudes of the signal change varied rather widely from one event to the next. In general, the characteristic behavior was a rather sharp initial change, followed by a trough (or crest), and then a gradual recovery. Invariably, the recovery was more rapid for the h-f signal.

Fig. 3 shows histograms of the number of coincidences between SWF of GLH and SSE of GLC during the period of the observations, and of GLH SWF over a longer period. Coincidences were observed only during the daylight hours when the h-f fades were more numerous.

Fig. 4 shows similar histograms of the number of GLH fades of intensity classified as "moderate" or greater and GLC enhancements which occurred during the same period of observation. This shows a high degree of correlation, so that the probability of a v-l-f enhancement is very high if the h-f effect is pronouced.

Fig. 5 represents a test to determine whether any correlation exists between the amplitude ranges of the v-l-f and h-f signals during an SID. The points are plotted with the increase in GLC signal (in decibels) as abscissa and the corresponding decrease (in decibels) of the GLH signal as ordinate. Points with an upward arrow attached correspond to complete fade-out of the GLH signal.

Examination of Fig. 5 shows that in no case was the GLC increase as great as that of the GLH decrease, and that no evident correlation between the magnitudes of the two effects exists. The largest GLC increase (14.1 db), for example, was associated with only a moderate fade on GLH. Conversely, the deepest fade of GLH (57.5 db) was accompanied by only a small increase (2.3 db) on GLC.

4. DISCUSSION

In the years since the observations described above were completed, a considerable body of information has accumulated concerning SID effects, solar

32

phenomena, and ionospheric structure. Observations of the type presented above, however, have not been published previously. It is of interest, therefore, to examine the results obtained in the light of present-day knowledge. In particular, it appears that these results have important implications on the type of solar event which causes the SID, and on the layer structure and responsive mechanisms in the upper atmosphere.

A plausible qualitative explanation for the h-f and v-l-f effects was advanced at an early date: The h-f waves are reflected by the E- and/or F-layers; absorption, however, takes place mainly in the intermediate D-region. V-l-f waves, on the other hand, undergo a waveguide type of propagation between the conducting earth and the conducting D-region, the attenuation depending on the conductivity of the guide "walls". Since an enhancement of D-region ionization should increase the "wall" conductivity, this will reduce the attenuation of v-l-f waves, but will give rise to increased absorption of h-f waves passing through the D-region.

It will be shown below that the above qualitative explanation must be modified and made more precise in order to fit the observations. In particular, it will appear that a sharpening of the lower boundary of the D-region must result from the flare. In order to bring this out, it is necessary to examine the absorption and reflection processes, as well as the changes in ionospheric layer characteristics, which take place as a result of a solar flare.

4.1 H-f Effects

Appleton and Piggott [7] have made a comprehensive study of h-f absorption at vertical incidence during a period extending over a sunspot cycle. They found that absorption was definitely under solar control, since it varied in a regular manner with solar zenith angle. They showed that the bulk of the absorption is of the non-deviative type, and that it must take place in a layer below the reflecting

33

level of the E-region. Furthermore, they showed that the absorbing region cannot be merely the lower portion of the E-region, but must be an independent ionized region, which they identify with the D-region.

The evidence which led Appleton and Piggott to the above conclusions was obtained from three types of behavior:

(1) The diurnal variations of absorption for two different frequencies, one of which is reflected by the E-layer and the other by the F-layer, have substantially the same dependence on the solar zenith angle.

(2) For a frequency whose reflection level shifts during the day from the F-layer to the E-layer, or to a sporadic E-layer, the absorption is the same for reflection from either layer (apart from the period when the frequency is in the neighborhood of fE, when additional deviative absorption takes place).

(3) The variation of absorption with frequency can be explained only on the assumption that the same medium is responsible for absorption over the entire frequency range.

For non-deviative absorption (i.e., in a region where the refractive index is substantially unity), Appleton [8] gave for the absorption coefficient κ in a region of ionization density N and collision frequency ν, under conditions where the quasi-longitudinal approximation holds,

$$\kappa = \frac{2\pi e^2}{mc} \frac{N\nu}{\nu^2 + (\omega \pm \omega_L)^2} \tag{1}$$

where ω_L is the magnitude of the longitudinal component of the angular gyro frequency, and the + sign is for the ordinary wave, the - sign for the extraordinary wave. The absorption of the ordinary wave is appreciably less than that of the extraordinary wave when ω/ω_L is not too large, so that it is the ordinary wave which then is measured. It can be seen that the dependence of κ on the collision frequency ν tends to a proportionality to either ν or $1/\nu$, depending on whether

34

v^2 is small or large compared with $(\omega + \omega_L)^2$. In the former case, the integrated absorption at vertical incidence for a wave which penetrates the absorbing region and is reflected (with negligible deviative absorption) at a higher level then is given by an expression of the form

$$\int \kappa \, ds = A(\omega + \omega_L)^{-2} \, F(\chi), \tag{2}$$

where A is a constant and $F(\chi)$ is a function of the solar zenith angle, χ, which depends on the rate and process by which free electrons disappear (e.g., recombination, attachment). Appleton and Piggott showed that the frequency dependence of the total absorption (as measured by an effective reflection coefficient) is in very good agreement with (2). This is shown by Fig. 6. Thus it follows that $v^2 \ll (\omega + \omega_L)^2$ throughout the absorbing region. Appleton and Piggott thus placed an upper limit for v of $2 \cdot 10^7/\text{sec}$ in the absorbing D-region.

Information regarding the electron production and removal processes in the absorbing region can be derived from a study of the dependence of absorption on the solar zenith angle χ. In particular, the theoretical relation shows that the effective reflection coefficient ρ depends on χ in a relation of the form

$$|\log \rho| \propto (\cos \chi)^n, \tag{3}$$

where n depends on the ionosphere model. For a Chapman layer (constant scale height and recombination coefficient), $n = 1.5$, while if the recombination coefficient is proportional to the ambient pressure, $n = 1.0$. Nicolet [9] showed that a region of mounting temperature with height would have a lower value of n than one of constant temperature.

The experimental values of n determined by Appleton and Piggott range from about 0.4 to 1.1. Taylor [10] found values from 0.7 to 1.30. Furthermore, Appleton and Piggott [7] found a winter anomaly, the absorption in winter being distinctly higher than for the same zenith angle at other seasons.

35

The experimental values, although not completely understandable on the basis of present theoretical knowledge, definitely show that the absorbing layer is not of the Chapman type (for which n = 1.5), and suggest that the region has a positive temperature gradient.

The above studies of ionospheric absorption have been concerned chiefly with vertically incident waves. Since the path length through the absorbing region increases as the secant of the angle of incidence on the absorbing layer, the types of variation described hold substantially for an oblique path of constant length.

It should be pointed out that Appleton and Piggott's findings relate to normal h-f absorption, and that the height region wherein the additional absorption during SID occurs cannot be localized from their measurements.

4.2 V-l-f Effects

Although the main features of h-f absorption are fairly well understood, this is not the case for v-l-f waves. The requisite theory is much more complicated, since variations in the properties of the important regions of the ionosphere take place in a distance comparable with a wavelength. This necessitates full wave theory, which is made complicated by the anisotropy of the medium. An analytical theory has been worked out only for special variations of electron density and critical frequency with height, and then only for the case of a vertical magnetic field or of vertical propagation. More recently, numerical procedures have been introduced to handle more general situations, but results are available only for a limited number of combinations of parameters.

Our present knowledge of D-region structure has been promoted by studies of the propagation characteristics of v-l-f waves. These characteristics will be summarized here in order to provide a background for the subsequent discussion of D-region mechanisms.

Although some measurements of layer height have been made at very low frequencies with pulse techniques (Brown and Watts [11], Helliwell [12], the Pennsylvania State University group [13]), the most extensive and detailed studies have been carried out on c-w transmissions, principally by English workers [14-22]. These measurements have been made at various distances extending out to about 1000 km.

The principal characteristics of the ionospherically propagated wave (the so-called "sky wave") are its phase, amplitude, and polarization. The phase depends on the length of the transmission path and the height of reflection. The apparent height of reflection is deduced from observation of the amplitude pattern versus distance produced by interference between the ground and sky waves, and also by measuring the phase difference between ground and sky waves for different frequencies. Variations in reflection height with time can be deduced from measurements of the phase variation of the sky wave at a given receiving point. For this purpose the sky wave is isolated from the ground wave by means of a special antenna arrangement. Observations of the change in phase of the sky wave are especially useful in testing solar control of the reflecting medium.

Measurements at a frequency of 16 kc/s, for example, show that a distinct change in the character of the sky wave takes place in the neighborhood of 400 km, corresponding to an angle of incidence on the ionosphere of about 65°. Consequently it will be convenient to discuss the short and long distance measurements separately, and then the modifications observed during SID.

4.2.1 Short Distance Characteristics

The measurements at short distances may be summarized as follows:

(a) Reflection Height

Typical results of the phase lag of the sky wave relative to

the ground wave are shown in Fig. 7. The height of reflection shows marked solar control during the day, in accordance with the relation

$$h = h_o + A(t) \log[Ch(\chi)], \tag{4}$$

where h_0 is the value corresponding to $\chi = 0$, and $Ch(\chi)$ is the Chapman function, which reduces to sec χ for χ less than about 85°. An average value of h_O is 73 ± 2 km. If reflection took place from a Chapman layer, the slope $A(t)$ of the height vs. log $[Ch(\chi)]$ curve would be the scale height. Fig. 8 shows curves of h_O and $A(t)$ at 16 kc/s through the course of the year. The apparent heights at noon and night near Cambridge, England are shown in Fig. 9. Values of $A(t)$ run around 6 km, which is a reasonable value for the scale height. Consequently this result was used for some time to infer that the reflecting layer was of the Chapman type. On 30 kc/s, however, a mean value is 5.5 ± 0.1 km, on 43 kc/s, 4.8 ± 0.1 km, and at 70 kc/s around 3 km, with greater variability at the higher frequencies. This variation of $A(t)$, however, is not explainable on the basis of a Chapman layer. It should be noted that the descent from the night-time height starts at a time very close to ground sunrise at the midpath point.

(b) Polarization

For short distances of 100-300 km, nearly all observations show that the sky wave on all frequencies from 16-150 kc/s is approximately circularly polarized with a left-handed sense of rotation. The polarization remains the same through an SID.

(c) Amplitude

In view of the approximately circular polarization of the sky wave, the components ρ_{22} and ρ_{12} of the tensor reflection coefficient [see Part I, p. 11] are approximately equal. The diurnal variation of the component ρ_{12}, called the "conversion coefficient", is shown in Fig. 10, and its seasonal variation in

38

Fig. 11, for a frequency of 16 kc/s. Fig. 12 shows the frequency trend of ρ_{12} for different seasons.

Figs. 13 and 14 show the diurnal variation of ρ_{12} on 16 and 70 kc/s, respectively, in summer and winter. It is seen that a pre-sunrise drop and post-sunset rise in amplitude takes place, with an essentially constant level during the day. (The small ripples in the winter daytime curve are considered as probably being due to a two-hop wave.) The drop in amplitude begins at a solar zenith angle of close to 98°.

It is evident that the daily amplitude variation is distinctly different from the daily height variation at short distances.

4.2.2 Long Distance Characteristics

The characteristics inferred from measurements over longer distances will be summarized in this section. These principally cover distances of about 400-950 km, but will also include some deductions made from observations over distances of several thousands of kilometers. These have been derived from four sources; (1) 16 kc/s observations at 540 km, (2) a series of observations over the Decca navigation chain at frequencies from 70 to about 130 kc/s, and distances up to 950 km, (3) phase variations at 16 kc/s and lower frequencies in connection with basic studies of navigation systems, and (4) observations of the v-l-f spectral characteristics of atmospherics.

(a) Reflection Height

The reflection heights determined from the ground interference pattern fit in with a reflection height of 70 ± 2 km at midday, with no apparent variation of height with frequency. This agrees within a few kilometers with the measurements near vertical incidence.

The diurnal variation of reflection height is illustrated by Fig. 15, for a

39

frequency of 16 kc/s. This is completely different from the diurnal variation at vertical incidence shown in Fig. 7. In fact, the height variation is very much like the amplitude variation near vertical incidence shown in Fig. 10. Similar types of variation were observed at higher frequencies, the sunrise drop in height being substantially complete at midpath around sunrise. This is shown in Fig. 16, for which it was assumed that the nighttime height was 90 km.

Pierce [23] reported a normal diurnal phase variation at 16 kc/s of $200^{\circ} \pm 30^{\circ}$ over a 5200 km path, while Casselman, Heritage, and Tibbals [24] measured a diurnal change of about $350^{\circ} \pm 30^{\circ}$ at 12.2 kc/s over a 4000 km path.

(b) Polarization

Measurements of the polarization of the sky wave showed this to be linear at about 45° to the vertical. This represents a change from the short distance measurements, which gave the polarization as approximately circular.

(c) Amplitude

The reflection coefficient at oblique incidence is found to be greater than at vertical incidence. For 16 kc/s, Bain, et al [19] found a value of 0.27 at summer midday, and 0.55 at night, compared to vertical incidence values of 0.15 and 0.50, respectively. For higher frequencies, Weekes and Stuart [21] obtained the results shown in Fig. 17. This shows an increasing reflection coefficient with distance, but smaller values at increasing frequency. Also, an increase of about 2:1 takes place between summer and winter.

The drop in amplitude around sunrise is shown in Fig. 18. This is similar to the behavior of the reflection height shown in Fig. 15, and to the amplitude behavior at short distances. Again, smaller values of reflection coefficient are found at the higher frequencies.

From measurements of v-l-f transmissions on available frequencies analyzed by

40

Eckersley [25], combined with observations of the spectrum of individual atmospherics, Chapman and Macario [26] deduced the attenuation vs. frequency curve shown in Fig. 19. This shows a minimum around 15 kc/s, and a maximum around 2 kc/s.

4.2.3 SID Effects

The effects of SID associated with solar flares have been observed both at the short and long distances used to obtain the results discussed above. In general, a change both in phase and amplitude of the sky wave is associated with an SID. The change in phase corresponds to a decrease in reflection height. This change in phase appears to be a very sensitive way to detect flares [27].

Near vertical incidence, the decrease in reflection height is substantially the same for frequencies in the range 16-135 kc/s. This is illustrated by Fig. 20(a). The amplitude near vertical incidence suffers a decrease during an SID, the change in amplitude being greater at higher frequencies, as shown in Fig. 20(b). The relative change in amplitude is roughly proportional to the decrease in reflection height, as shown by Fig. 21 for 16 kc/s.

The above characteristics, observed near vertical incidence, undergo a drastic change at oblique incidence associated with the longer ranges (>500 km). The phase change associated with the reduction in height of reflection decreases with increasing frequency, while the amplitude increases markedly. The amount of this increase is greater, for example, at 70 kc/s than at higher frequencies. Fig. 22 shows an example of the relative phase and amplitude changes observed at a distance of about 900 km during an SID. From observations of SEA, it appears that the amplitude increase may be a maximum for frequencies around 30 kc/s.

Pierce [23] showed an example of a phase advance at 16 kc/s over a 5200 km path during an SID. This SID, of importance 3, accompanied a solar flare of importance 2+.

41

A phase advance of 100° was observed. This is half the normal diurnal change, or equivalent to a reduction in height of reflection of about 9 km. No amplitude change was observed, however. On the other hand, during a 3- SID, accompanying a 2 flare, a 60 kc/s signal over the same path experienced a phase advance of only 70°, corresponding to a height change of about 1.6 km, while the amplitude increased considerably. Pierce suggested that the primary physical phenomenon produced by the SID might be a steepening of the ionization gradient, with an accompanying reduction in the phase lag at reflection.

Gardner [28] and Obayashi, et al [29,30] showed that an SID shifted the __equency spectrum of atmospherics upwards, so that the frequency of minimum attenuation was raised. Also, the low-frequency cutoff of the ionospheric waveguide was raised, corresponding to a decrease in height of the reflecting region.

To summarize the SID effects observed on v-l-f wave propagation, the SID produces a reduction in reflection height and a change in amplitude of the sky wave. Near vertical incidence the reduction in reflection height appears to be substantially independent of frequency, while the amplitude change is a decrease. The amount of this decrease is progressively greater at higher frequencies, and roughly proportional to the decrease in reflection height. At 100 kc/s the decrease may be by a factor of about 100. At oblique incidence, on the other hand, the decrease in reflection height is less for higher frequencies, while the sky wave amplitude increases markedly. This increase, which may be by a factor of 5 or more, appears to be a maximum at frequencies around 30 kc/s, and becomes less for higher frequencies.

4.2.4 Eclipse Effects

Observations of the phase of the sky wave on 16 kc/s at steep incidence were made during a partial solar eclipse by Bracewell [31]. Although the

42

greatest eclipsed area was only 0.3 of the solar disk, a definite phase anomaly was found, as shown in Fig. 23. The form can be seen to agree roughly with the shape of the obscured area curve.

From this result, Bracewell deduced that the relaxation time of the reflecting region probably did not exceed 6 minutes. Furthermore, the magnitude of the phase change -- about 35 degrees -- represented an increase in height of reflection of about 1 km, while for a Chapman layer a change of only about 0.2 km would be expected.

4.3 D-Layer Production and Structure

A proper interpretation of SID effects on ionospheric propagation ultimately requires a knowledge of the composition of the ionizing agents, and of the reactions which lead to the prevailing ionization densities. In this Section, some of the pertinent available information will be summarized.

4.3.1 The Two-Layer Model

In order to explain the diurnal phase and amplitude variations discussed in Sec. 4.2.1 and 4.2.2, Bracewell and Bain [32] proposed an ionospheric model containing a two-layer D-region. The height of the upper layer, which they denoted by $D\alpha$, was supposed to be under solar control in accordance with the formula

$$h = 72 + 5.5 \log \sec \chi \text{ km.} \tag{5}$$

This is shown by the upper curve in Fig. 24. Below this layer, a layer denoted by $D\beta$ was postulated to exist, with height variations as shown in the lower part of Fig. 24. The upper layer was supposed to be the reflecting layer for 16 kc/s waves at steep incidence, while the lower layer was considered to be responsible for absorption of the waves. At sufficiently glancing incidence, however, reflection would take place at the lower layer.

Bracewell and Bain based their two-layer model entirely on the observations of

43

16 kc/s propagation at short and medium distances. They gave no suggestions as to the mechanisms by which these two layers could be formed.

4.3.2 Bracewell's Exhaustion Region

In order to explain the observed type of solar flare and eclipse effects on the D-region, Bracewell [31] postulated the existence of a so-called "exhaustion region", in which the ionizable constituent exists in a small concentration. With respect to a two-layer D-region, this mechanism was supposed to take place in the upper region, denoted by D_u in Sec. 4.3.1.

Bracewell showed that an exhaustion region would explain the amount of change in reflection height observed during a partial solar eclipse, whereas a much smaller change would result from a Chapman region. He also showed that an exhaustion region would produce h-f absorption whose variation with $\cos \chi$ agreed in general with experimental observations.

Bracewell also showed that the characteristics of an exhaustion region would explain satisfactorily the observed reductions in reflection height during solar flares. For example, a reduction of 15 km in height would require an increase in intensity of the incident ionizing radiation by a factor of 15. However, no attempt was made to deduce the accompanying effect on the amplitude of v-l-f waves.

4.3.3 Ionization Mechanisms

The existence of several separate mechanisms for the formation of ionization in the D-region has been brought out in the last decade or so. Brown and Petrie [32], pursuing a suggestion attributed to Ratcliffe, have evaluated the role of photodetachment of electrons from O_2^- ions. This ion, formed by the attachment of an electron to a neutral oxygen molecule, starts building up in concentration around sunset, resulting in the disappearance of the normal D-layer. The nighttime level of ionization below the E-layer is maintained by cosmic rays, which vary in

44

intensity with latitude. Visible light, extending down into the infrared, can supply the energy required to break up the attachment, and thus liberate free electrons. Since visible light can reach the altitudes >50 km appreciably before ground sunrise, electrons released by the photodetachment process build up D-layer ionization appreciably before sunrise. Brown and Petrie [33], and Moler [34] showed that this explained satisfactorily the pre-sunrise drop in amplitude discussed in Sec. 4.2.1. Aiken [35] verified the fact that a two-layer D-region would be produced at sunrise, the lower layer being due to cosmic rays, and the upper layer to photoionization of nitric oxide by Lyman-α radiation. Thus, in the two-layer model of Bracewell and Bain discussed in Sec. 4.3.1, these mechanisms would account for the layers $D\beta$ and $D\alpha$, respectively.

Nicolet and Aikin [36], in a discussion of the formation of the D-region, pointed out the following mechanisms of ionization which are possible at levels below 85 km:

> (1) X-rays of $\lambda < 10$ A;
>
> (2) Lyman-α radiation ($\lambda = 1215.7$A);
>
> (3) Ultraviolet radiation, $\lambda > 1800$ A;
>
> (4) Cosmic rays;
>
> (5) Photodetachment by visible radiation.

The normal E-layer, which is ascribed to the combined affect of soft X-rays in the range 30-100 A and ultraviolet radiation (Lyman-β) is penetrated by cosmic rays, ultraviolet radiation of $\lambda > 1800$ A, Lyman-α and hard X-rays ($\lambda < 10$ A).

Of these, cosmic rays and hard X-rays are capable of ionizing all atmospheric constituents. In addition, Lyman-α, due to a narrow window in O_2 absorption at the Lyman-α line, can penetrate to low levels. A minor constituent, NO (≈ 1 part in 10^{10} was proposed by Nicolet [37] as the ionizable constituent responding to Lyman-α to

account for the daytime D-layer.

In view of the presently-accepted view that the upper part of the D-region, $D\alpha$, is due to photoionization of NO by Lyman-α, it is tempting to suppose that NO is the ionizable constituent responsible for the exhaustion region postulated by Bracewell. The concentration of NO has been estimated by Nicolet [38] as about 10^{-10} of the total concentration below about 85 km, or about 10^5 cm^{-3} at 75 km [36]. In order to give ionization densities to fit the v-l-f observations, however, the NO concentration would have to be lower than this by about two orders of magnitude, or about 10^3 cm^{-3} at 75 km.

Although Bracewell believed the exhaustion region would also explain solar flare effects, this must be rejected on the basis of later evidence. For example, Friedman and collaborators [39] observed no large increases in Lyman-α during flares, whereas Bracewell requires a factor of about 15. In a recent report, Chubb, et al [40] stated that no increase in Lyman-α occurred during a l+ flare, but X-rays in the range 1-10 A were observed. As mentioned earlier, the solar flare enhancement of ionization has been shown to be explainable by the appearance of hard X-rays in the wavelength range 1-10 A, which ionize all atmospheric constituents, and can penetrate to low levels because of the low absorption coefficients in this spectral region. The resulting ionization would be even less sharply distributed in height than a Chapman region.

4.4 Comparison With SID Results

The two features of the experimental results shown in Fig. 5 which require explanation are the following:

    (1)   The lack of correlation between the magnitudes of SWF and SSE;

    (2)   The mechanism which produces the SSE.

It will now be shown that the first is explainable on the basis of D-layer structure

and solar flare radiation, but that an adequate explanation of the second is not available on the basis of present knowledge.

4.4.1 Absence of Correlation Between Magnitudes of SWF and SSE

The absence of any correlation between SWF and SSE in Fig. 5 is understandable within the framework of the two-layer model discussed in Sec. 4.3.1. For example, if the flare produces a burst of hard X-rays without any enhancement in Lyman-α radiation, then both the regions of the $D\alpha$ and $D\beta$ layers will be intensified. The relative intensifications of these two regions will depend on the spectral distribution of the X-radiation. There is no reason to believe, at present, that all solar flares have the same spectral distribution, so that the relative increases can be expected to change from flare to flare. The increase in h-f absorption leading to SWF is the sum of the increases in the two regions, while the v-l-f SSE would respond only to changes in the lower layer, $D\beta$. Consequently, this would result in the absence of any clear-cut statistical correlation between the v-l-f and h-f effects of flares.

4.4.2 Mechanisms Associated With SSE

The observations reported in Sec. 3 show that SSE on vlf is one of the phenomena accompanying SID produced by solar flares. It was also stated that such enhancements can be understood in a qualitative way as due to reduced normal-mode attenuation as a result of increased conductivity of the ionosphere, acting as the upper wall of a waveguide. It will now be shown that this qualitative explanation cannot be substantiated on the basis of presently accepted ionization processes and present theoretical knowledge concerning v-l-f propagation.

For the ranges involved in the observations reported here, the normal-mode theory of propagation is more advantageous than the ray theory, since only one mode is effective. A number of analytical treatments of this theory have appeared [41-55],

47

but none treats the problem in a sufficiently general way to allow definitive conclusions to be drawn pertinent to the present observations. Analytical solutions have been obtained only for special distributions of ionization density and collision frequency with height, and for special directions of the earth's magnetic field (usually taken to be vertical). Because of the inability to produce an analytical solution of sufficient generality, efforts have been directed towards obtaining numerical solutions [56-60]. This approach is not restricted to special height distributions, but a very large number of special cases needs to be worked out in order to produce a sufficiently extensive catalog from which deductions of a general nature can be drawn. As yet, only a rather small number of examples has been worked out, so that the results from which one must draw general inferences are rather scanty. Nevertheless, these tend to show that, other things remaining unchanged, the attenuation decreases as the ionosphere boundary becomes sharper. Also, for a constant collision frequency, the attenuation decreases as the height of the boundary decreases.

One of the idealizations which reduces greatly the complexity of the calculations is that of a sharply bounded homogeneous ionosphere. Calculations using such a model have been made, among others, by Spies and Wait [53], under the further assumption that the quasi-longitudinal approximation of Booker [61] may be used. The ionospheric parameters then enter the analysis in an effective conductivity ω_r given by

$$\omega_r = \frac{\omega_N^2}{(\nu^2 + \omega_L^2)^{1/2}} \tag{6}$$

where ω_N, ν, ω_L are the plasma, collision, and longitudinal gyro angular frequencies, respectively.

Fig. 25 (from [53]) shows the attenuation of the first mode in db/1000 km as a function of frequency for various ionosphere heights for a value of ω_r of $2 \cdot 10^5$.

48

It can be seen from these curves that a reduction of height from 75 to 60 km, say, would result in a reduction of slightly more than 0.2 db/1000 km for a frequency of 30 kc/s. For a 5400 km path, the total reduction in attenuation would be about 1.2 db, if the height reduction occurred uniformly over the whole path. This attenuation decrease is the result of a decrease in the grazing angle of the first mode to the ionosphere. However, this decrease in attenuation is based on a constant effective conductivity, ω_r, so that the collision frequency, ν, is assumed to remain unchanged.

The electron density distributions in the D-region shown in Fig. 26, calculated by Nicolet and Aiken [36], show no appreciable change in shape at a density of about 10^3 cm^{-3} between a quiet sun and a strong flare. Consequently, a solar enhancement will cause a given ionization density to appear at a lower level, but with substantially the same gradient. Hence one might argue that it is reasonable to suppose that a decrease in attenuation as a result of a decrease of 15 km in reflection height of the same order as that calculated for the sharply bounded ionosphere would occur. However, in virtue of the approximately exponential increase in critical frequency with such a height decrease, the value of ω_r, the effective ionosphere conductivity, would be decreased. On the basis of Kane's [62] measurement of collision frequency, a 15 km height decrease would bring about an increase in ν of a factor of 10. Assuming a value of ω_L of about $5 \cdot 10^6$ as a representative value for the transatlantic path in the measurements with which we are concerned, then the effective conductivity would decrease by a factor of about 2.3. Thus the qualitative expectation of an enhanced ionospheric conductivity would not be realized. Instead, an appreciable decrease in effective conductivity would result.

The above conclusion, it must be emphasized, is, at most, semi-quantitative, since it is based on the behavior of an idealized sharply bounded ionosphere having

49

"average" properties given by the Nicolet and Aiken results.

In order to obtain an increased conductivity at the lowered heights due to
the onset of a flare, an increased gradient at these lower heights appears to be
required. In other words, in addition to increasing the ionization densities at
all levels in the D-region, it appears that the flare must increase the sharpness
of the lower boundary. This would result in a decreased penetration of the waves
reflected therefrom, and hence, for a sufficiently sharp boundary, could outweigh
the effect of the increased collision frequency encountered at the lowered reflec-
tion height. Again, it must be emphasized that this line of argument is only
qualitative, and that an adequate quantitative theory is needed before a firm con-
clusion can be reached.

If we grant, for the time being, that an increased sharpness of the lower
boundary of the D-layer is required to explain the SSE produced by the flare, then
it is necessary to adduce the mechanism which produces this effect. As mentioned
above, the electron density distributions calculated by Nicolet and Aiken, which
are shown in Fig. 26, show no appreciable change in shape at the electron densities
required.

5. CONCLUSIONS

Simultaneous observations of short-wave fade-outs (SWF) of a 13.5-Mc/s
signal and sudden signal enhancements (SSE) of a 31.15-kc/s signal over substantially
the same transatlantic path of approximately 5400 km show no evident correlation
between the magnitudes of the two effects of the SID. This absence of correlation
is understandable on the basis of a two-layer D-region. The lower layer is produced
by cosmic rays, while the upper layer is due to photoionization of nitric oxide by
Lyman-α radiation. Hard X-rays (in the range 1-10 A) emitted by a solar flare

penetrate to the low levels of the D-region and ionize all constituents (principally O_2 and N_2). The relative intensifications of the two D-regions will depend on the spectral distribution of the X-radiation. On the assumption that the spectral distribution varies from flare to flare, the relative increases also can be expected to vary from flare to flare. Since the increase in h-f absorption is the sum of the increases in the two regions, while the v-l-f enhancement is occasioned only by the changes at the lower level, no correlation should result between the two effects.

On the other hand, an adequate explanation of the mechanism of the v-l-f enhancement is not available on the basis of present knowledge. Phase measurements show that a definite decrease in height of the lower boundary of the D-region is caused by the flare. This reduced height causes reflection to take place at a level of higher collision frequency, which should result in a decrease in the effective conductivity of the layer if the ionization gradient remains the same. Consequently, it appears that an increase in the sharpness of the lower boundary of the D-region is required during the onset of a solar flare. The mechanism by which this takes place needs to be determined.

51

6. BIBLIOGRAPHY

[1] H. Mögel, "Über die Beziehungen zwischen Empfangs-Störungen bei Kurzwellen und den Störungen des magnetischen Feldes der Erde", Telefunken Zeit., V. 11, pp. 14-31, 1930.

[2] J. H. Dellinger, "Sudden disturbances of the ionosphere", Proc. I.R.E., V. 25, pp. 1253-1290, 1937.

[3] R. Bureau & J. Maire, "Anomalies ionospheriques a debut brusque", Comptes Rendus (Paris), V. 203, pp. 1275-1278, 1936.

[4] K. G. Budden and J. A. Ratcliffe, "An effect of catastrophic ionospheric disturbances on low-frequency radio waves", Nature, V. 140, pp. 1060-1061, 1937.

[5] R. Bureau, "Effect of catastrophic disturbances on low-frequency radio waves", Nature, V. 141, p. 646, 1938.

[6] M. Katzin and A. M. Braaten, "Observations of very-low-frequency propagation during sudden ionospheric disturbances", presented at the joint meeting of the International Scientific Radio Union and the Institute of Radio Engineers, Washington, D. C., Oct. 20, 1947.

[7] E. V. Appleton and W. R. Piggott, "Ionospheric absorption measurements during a sunspot cycle", Jour. Atmos. & Terr. Phys., V. 5, pp. 141-172, 1954.

[8] E. V. Appleton, "Regularities and irregularities in the ionosphere - I", Proc. Roy. Soc., A, V. 162, pp. 451-479, 1937.

[9] M. Nicolet, "Effects of the atmospheric scale height gradient on the variation of ionization and short wave absorption", Jour. Atmos. & Terr. Phys. V. 1, pp. 141-146, 1954.

[10] E. W. Taylor, "Absorption of radio waves reflected at vertical incidence
      as a function of the sun's zenith angle", Jour. Res. NBS, V. 41,
      pp. 575-579, 1948.

[11] J. N. Brown and J. M. Watts, "Ionosphere observations at 50 kc", Jour. Geoph.
      Res., V. 55, pp. 179-181, 1950.

[12] R. A. Helliwell, "Ionospheric virtual height measurements at 100 kc/s",
      Proc. I.R.E., V. 37, pp. 888-894, 1949.

[13] A. H. Waynick, "Studies of the ionosphere using very long wave pulse
      techniques", ICSU Mixed Commission on Ionosphere, Proc. of Second Meeting,
      pp. 161-165, 1951.

[14] J. E. Best, J. A. Ratcliffe, and M. V. Wilkes, "Experimental investigation
      of very long waves reflected from the ionosphere", Proc. Roy. Soc., A,
      V. 156, pp. 614-633, 1936.

[15] K. G. Budden, J. A. Ratcliffe, and M. V. Wilkes, "Further investigations of
      very long waves reflected from the ionosphere", Proc. Roy. Soc., A, V. 171,
      pp. 188-214, 1939.

[16] K. Weekes, "The ground interference pattern of very-low-frequency waves",
      Proc. I.E.E., V. 97, Pt. IV., pp. 100-107, 1950.

[17] T. W. Straker, "The ionospheric propagation of radio waves of frequency 16 kc/s
      over short distances", Proc. I.E.E., V. 102, Pt. C, pp. 122-133, 1955.

[18] R. N. Bracewell, "The ionospheric propagation of radio waves of frequency
      16 kc/s over distances of about 200 km", Proc. I.E.E., V. 99, Pt. IV.,
      pp. 217-229, 1952.

[19] W. C. Bain, R. N. Bracewell, T. W. Straker, and C. H. Westcott, "The ionos-
      pheric propagation of radio waves of frequency 16 kc/s over distances of
      about 550 km", Proc. I.E.E., V. 99, Pt. IV., pp. 250-259, 1952.

[20] R. N. Bracewell, J. Harwood, and T. W. Straker, "The ionospheric propagation of radio waves of frequency 30-65 kc/s over short distances", Proc. I.E.E., V. 101, Pt. IV., pp. 154-162, 1954.

[21] K. Weekes and R. D. Stuart, "The ionospheric propagation of radio waves with frequencies near 100 kc/s over short distances", Proc. I.E.E., V. 99, Pt. IV., pp. 29-37, 1952.

[22] K. Weekes and R. D. Stuart, "The ionospheric propagation of radio waves with frequencies near 100 kc/s over distances up to 1000 km", Proc. I.E.E., V. 99, Pt. IV., pp. 38-46, 1952.

[23] J. A. Pierce, "VLF phase shifts associated with the disturbance of February 23, 1956", Jour. Geoph. Res., V. 61, pp. 475-483, 1956.

[24] C. J. Casselman, D. P. Heritage, and M. L. Tibbals, "Propagation measurements for the Radux-Omega navigation system", Proc. I.R.E., V. 47, pp. 829-839, 1959.

[25] T. L. Eckersley, "Studies in radio transmission", Jour. I.E.E., V. 71, pp. 405-454, 1932.

[26] F. W. Chapman and R. C. V. Macario, "Propagation of audio-frequency radio waves to great distances", Nature, V. 177, pp. 930-933, 1956.

[27] R. N. Bracewell and T. W. Straker, "The study of solar flares by means of very long radio waves", M.N.R.A.S., V. 109, pp. 28-45, 1949.

[28] F. F. Gardner, "The use of atmospherics to study the propagation of very long radio waves", Phil. Mag., V. 41, pp. 1259-1269, 1950.

[29] T. Obayashi, S. Fujii, and T. Kidokorc, "An experimental proof of the mode theory of VLF ionospheric propagation", Jour. Geomag. & Geodec. V. 10, pp. 47-55, 1959.

[30] T. Obayashi, "Measured frequency spectra of very-low-frequency atmospherics", Jour. Res. NBS-D. Radio Propagation, V. 64D, pp. 41-48, 1960.

[31] R. N. Bracewell, "Theory of formation of an ionospheric layer below E layer based on eclipse and solar flare effects at 16 kc/sec", Jour. Atmos. & Terr. Phys., V. 2, pp. 226-235, 1952.

[32] R. N. Bracewell and W. C. Bain, "An explanation of radio propagation at 16 kc/sec in terms of two layers below E layer", Jour. Atmos. & Terr. Phys., V. 2, pp. 216-225, 1952.

[33] S. B. Brown and W. Petrie, "The effect of sunrise on the reflection height of low frequency waves", Can. Jour. Phys., V. 32, pp. 90-98, 1954.

[34] W. F. Moler, "VLF propagation effects of a D-region layer produced by cosmic rays", Jour. Geoph. Res., V. 65, pp. 1459-1468, 1960.

[35] A. C. Aiken, "A preliminary study of sunrise effects in the D-region", Penn. State Univ. Ionosphere Res. Lab., Sci. Rep. No. 133, June 1, 1960.

[36] M. Nicolet and A. C. Aiken, "The formation of the D-region of the ionosphere", Jour. Geoph. Res., V. 65, pp. 1469-1483, 1960.

[37] M. Nicolet, "Contribution à l'étude de la structure de l'ionosphère", Mem. Inst. Roy. Met. Belg., No. 19, pp. 83-244, 1945.

[38] M. Nicolet, "Aeronomic chemical reactions", Symposium on Upper Atmosphere and Medicine, San Antonio, Nov. 1958.

[39] J. A. Ratcliffe, ed., "Physics of the Upper Atmosphere", p. 199, Academic Press, New York, 1960.

[40] T. A. Chubb, H. Friedman, R. W. Kreplin, W. A. Nichols, A. E. Unzicker, and M. J. Votaw, "Solar Radiation Satellite, IGY Bull. No. 42, Trans. A.G.U., V. 41, pp. 717-721, 1960.

[41] M. V. Wilkes, "The theory of reflexion of very long wireless waves from the ionosphere", Proc. Roy. Soc., A, V. 175, pp. 143-163, 1940.

[42] M. V. Wilkes, "The oblique reflexion of very long wireless waves from the ionosphere", Proc. Roy. Soc. A, V. 189, pp. 130-147, 1947.

[43] J. P. Stanley, "The absorption of long and very-long waves in the ionosphere", Jour. Atmos. & Terr. Phys., V. 4, pp. 65-72, 1950.

[44] K. G. Budden, "The propagation of a radio-atmospheric", Phil. Mag., V. 42, pp. 1-19, 1951.

[45] K. G. Budden, "The reflection of very low frequency radio waves at the surface of a sharply bounded ionosphere with superimposed magnetic field", Phil. Mag., V. 42, pp. 833-850, 1951.

[46] J. Heading and R. T. P. Whipple, "The oblique reflexion of long wireless waves from the ionosphere at places where the earth's magnetic field is regarded as vertical", Phil. Trans. Roy. Soc., A, V. 244, pp. 469-503, 1952.

[47] J. Heading, "The reflexion of vertically-incident long radio waves from the ionosphere when the earth's magnetic field is oblique", Proc. Roy. Soc., A, V. 231, pp. 414-435, 1955.

[48] Ya. L. Al'pert, "Low frequency electromagnetic wave propagation over the surface of the earth". Moscow (1955).

[49] J. R. Wait, "The mode theory of VLF ionospheric propagation for finite ground conductivity", Proc. I.R.E., V. 45, pp. 760-767, 1947.

[50] J. R. Wait, "An extension to the mode theory of VLF ionospheric propagation", Jour. Geoph. Res., V. 63, pp. 125-135, 1958.

[51] J. R. Wait, "Terrestrial propagation of very-low-frequency radio waves. A theoretical investigation", Jour. Res. NBS-D. Radio Propagation, V. 64D, pp. 153-204, 1960.

[52] J. R. Wait and K. Spies, "Influence of earth curvature and the terrestrial magnetic field on VLF propagation", Jour. Geoph. Res., V. 65, pp. 2325-2331, 1960.

[53] K. P. Spies and J. R. Wait, "Mode calculations for VLF propagation in the

earth-ionosphere waveguide", NBS Tech. Note No. 114, U.S. Dept. of Com.,
Off. of Tech. Serv., 1961.

[54] J. R. Wait, "A new approach to the mode theory of VLF propagation", Jour.
Res. NBS-D. Radio Propagation, V. 65D, pp. 37-46, 1961.

[55] J. R. Wait, "On the propagation of VLF and ELF radio waves when the ionos-
phere is not sharply bounded", Jour. Res. NBS-D. Radio Propagation,
V. 66D, pp. 53-61, 1962.

[56] K. G. Budden, "The numerical solution of differential equations governing
reflexion of long radio waves from the ionosphere", Proc. Roy. Soc., A,
V. 227, pp. 516-537, 1955.

[57] K. G. Budden, "The numerical solution of differential equations governing
reflexion of long radio waves from the ionosphere. II", Phil. Trans. Roy.
Soc., A, V. 248, pp. 45-72], 1955.

[58] D. W. Barron and K. G. Budden, "The numerical solution of differential
equations governing reflexion of long radio waves from the ionosphere. III",
Proc. Roy. Soc., A, V. 249, pp. 387-401, 1959.

[59] D. W. Barron, "The 'waveguide mode' theory of radio wave propagation when the
ionosphere is not sharply bounded", Phil. Mag., V. 4, pp. 1068-1081, 1959.

[60] D. W. Barron, "The numerical solution of differential equations governing
reflexion of long radio waves from the ionosphere. IV", Proc. Roy. Soc., A,
V. 260, pp. 393-408, 1961.

[61] H. G. Booker, "The application of the magneto-ionic theory to the ionosphere",
Proc. Roy. Soc., A, V. 150, pp. 267-286, 1935.

[62] J. A. Kane, "Arctic measurements of electron collision frequencies in the
D-Region of the Ionosphere", Jour. Geoph. Res., V. 64, pp. 133-139, 1959.
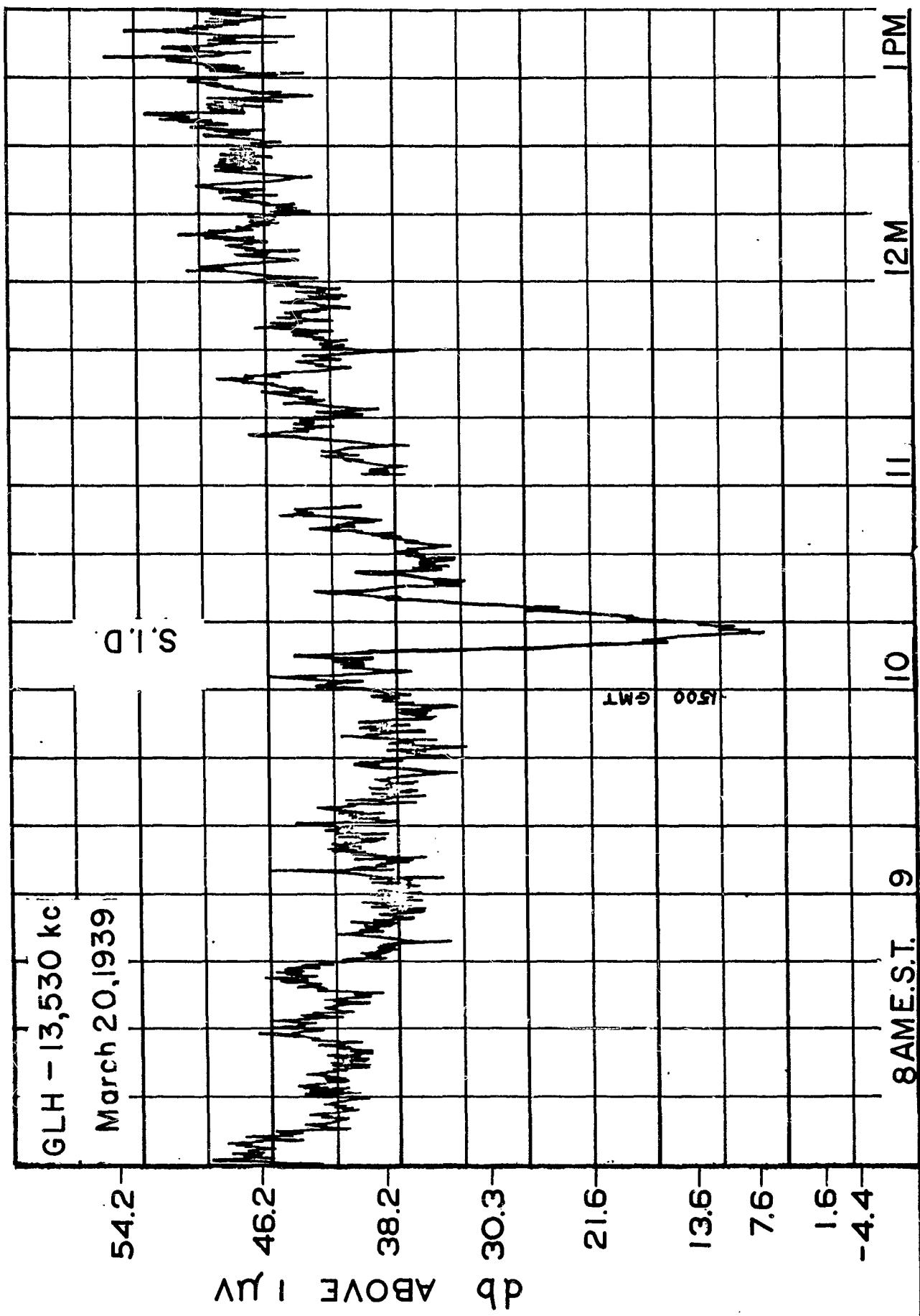
Fig. 1.—Record of GLH signal showing fade due to SID at 1510 U.T., March 20, 1939.
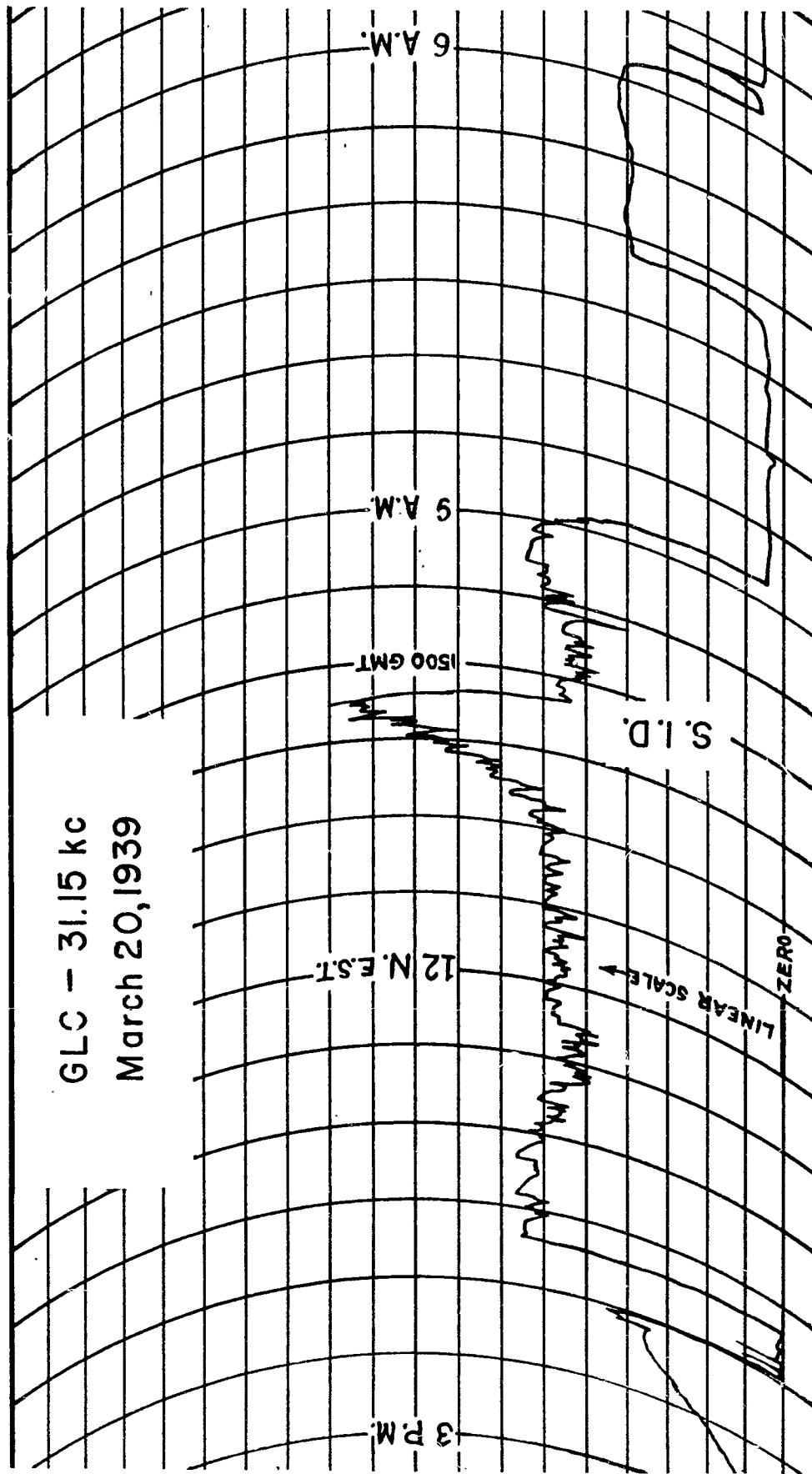
Fig. 2—Record of GLC signal showing enhancement due to SID at 1510 U.T., March 20, 1939.
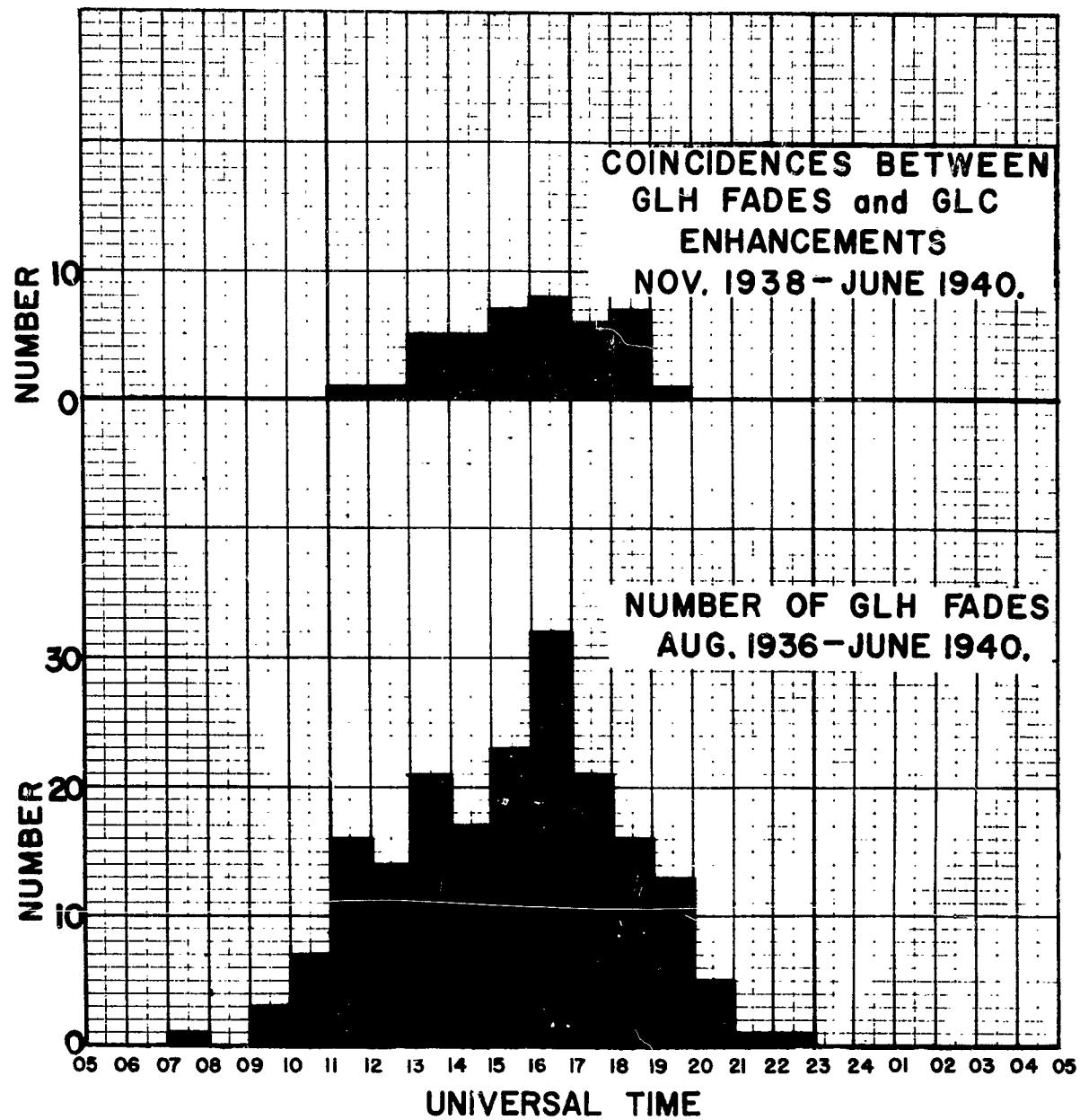
Fig. 3—Histogram of GLH fades, and of coincidences
between GLH fades and GLC enhancements.
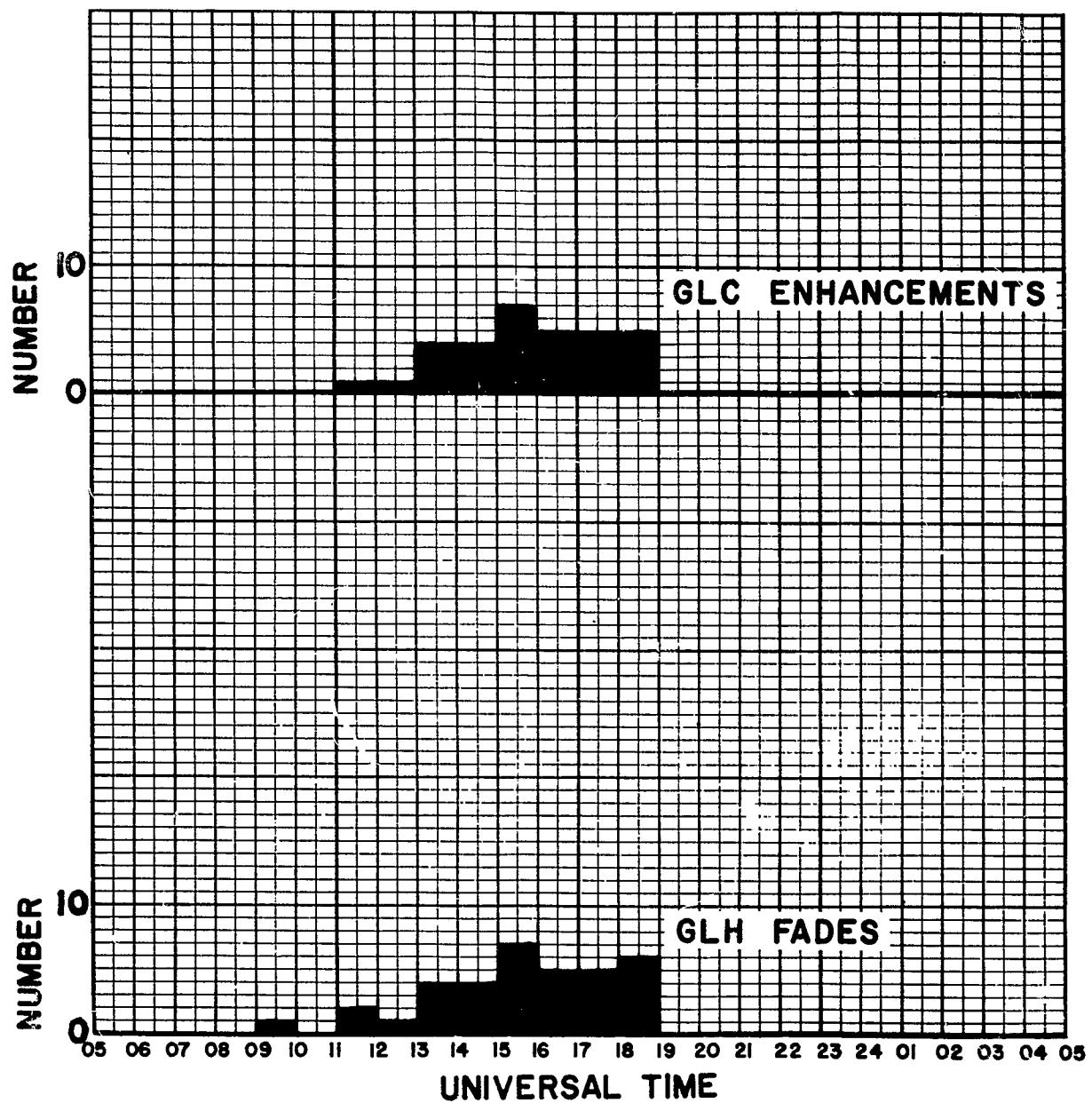
Fig. 4--Histograms of GLC enhancements and GLH fades of
intensity "moderate" or greater, during common
operating periods.

61
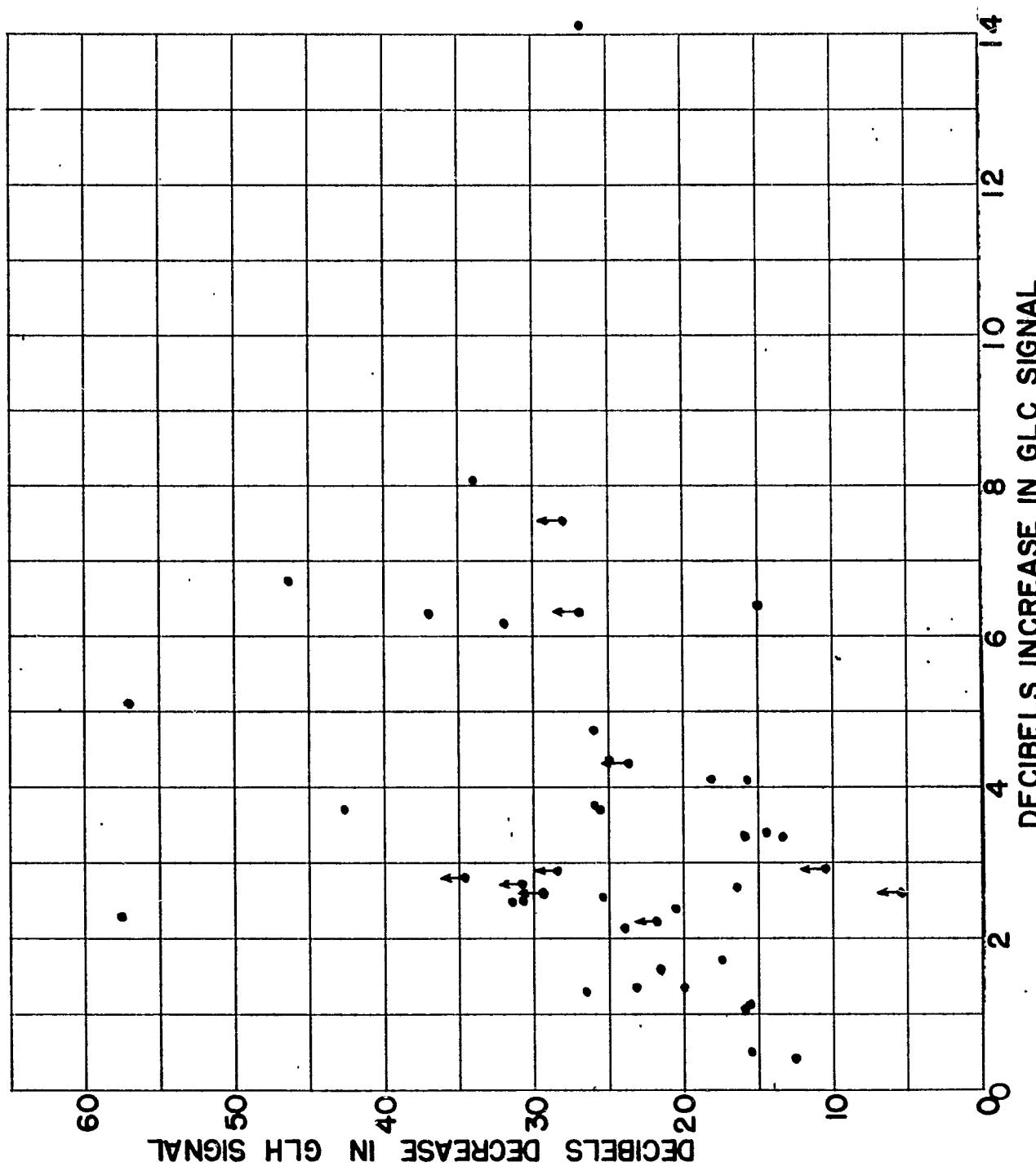
Fig. 5—Correlation plot of decrease in GLH signal vs. increase in GLC signal.
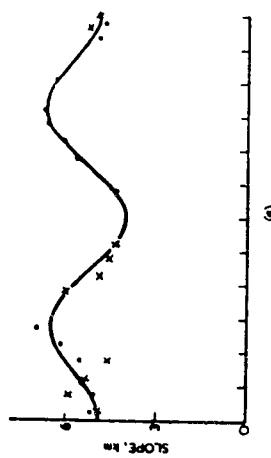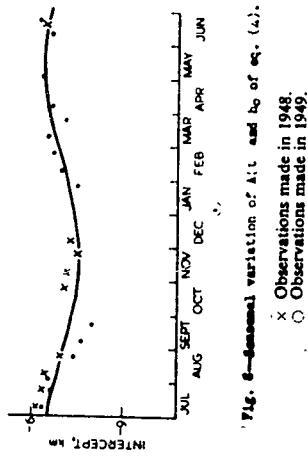
Fig. 5—Seasonal variation of $A.t.$ and t_0 of eq. (4).

× Observations made in 1948.
○ Observations made in 1949.
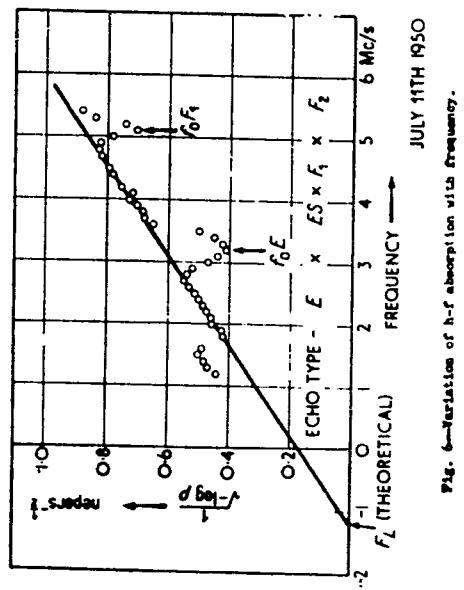
Fig. 6—Variation of h.f absorption with frequency.
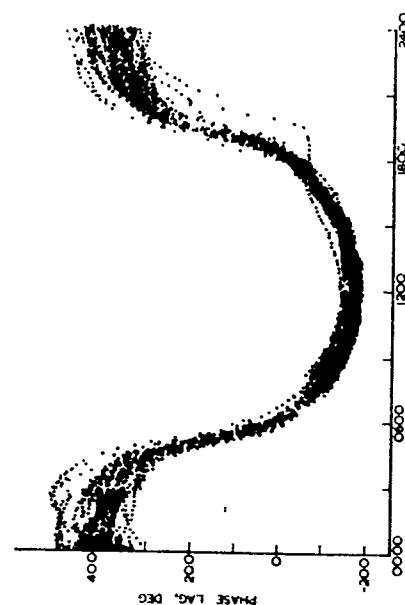
Fig. 7—Diurnal variation of horizontally-polarised component of sky wave: 28 June–7 August, 1948.
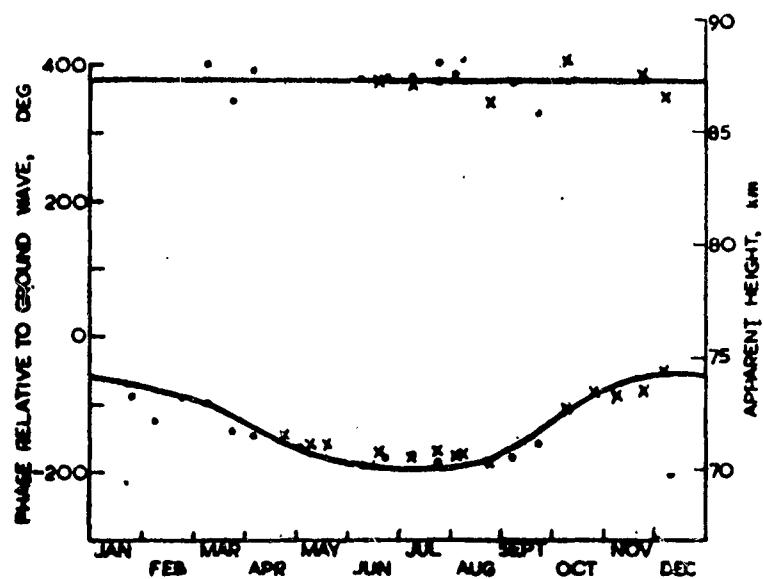
Fig. 9— Seasonal variation of the apparent height of reflection at night (upper curve) and at local noon (lower curve).

× Observations made in 1948.
○ Observations made in 1949.
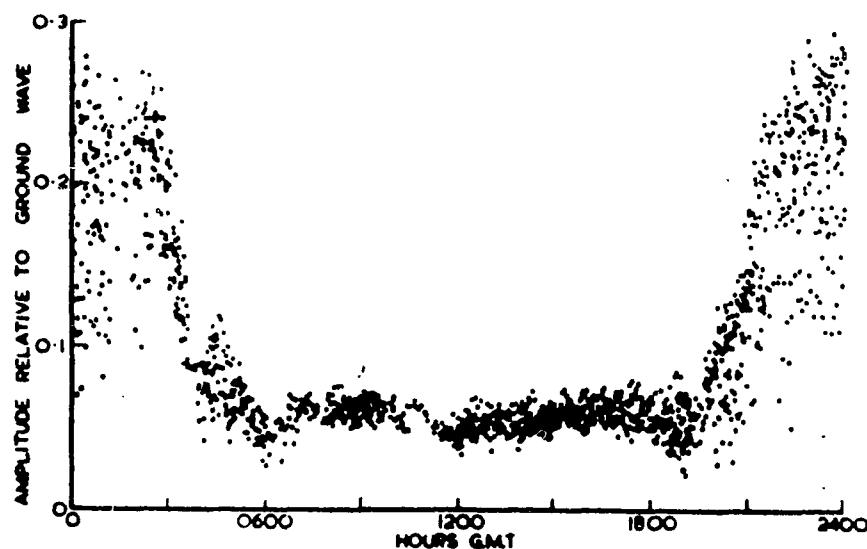
Fig. 10—Diurnal variation of conversion coefficient p_{12} on 16 kc/s, 2-15 July, 1948.
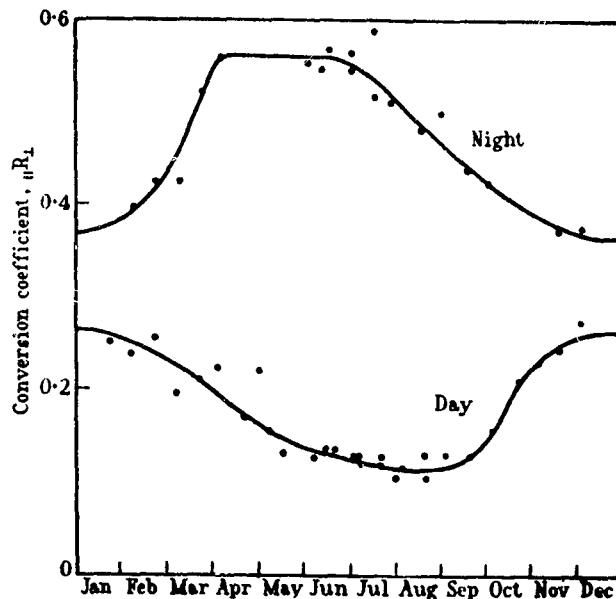
Fig. 11— The seasonal variation of ρ_{12} observed on a frequency of 16 kc/s for midnight (upper curve) and midday (lower curve).

● ● ● Represents observations made in 1948
○ ○ ○ Represents observations made in 1949.
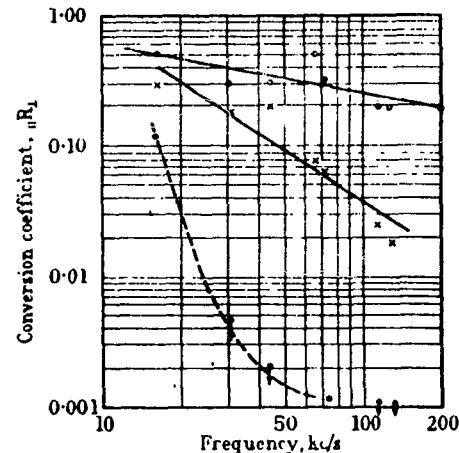
Fig. 12—The variation of conversion coefficient ρ_{12} with frequency for different seasons.

○ ○ ○ Winter night.
× × × Winter noon.
● ● ● Summer noon.
↓ ↓ ↓ Represents an upper limit when measurements are confused by noise.
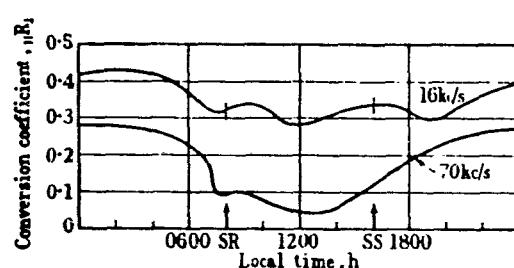
Fig. 13— The daily variation of ρ_{12} in winter as observed on 16 kc/s (upper curve) and 70 kc/s (lower curve).
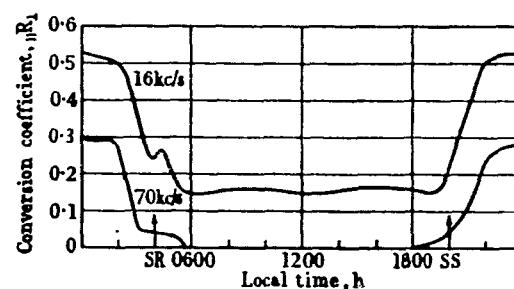
Fig. 14—The daily variation of ρ_{12} in midsummer as observed on 16 kc/s (upper curve) and 70 kc/s (lower curve).
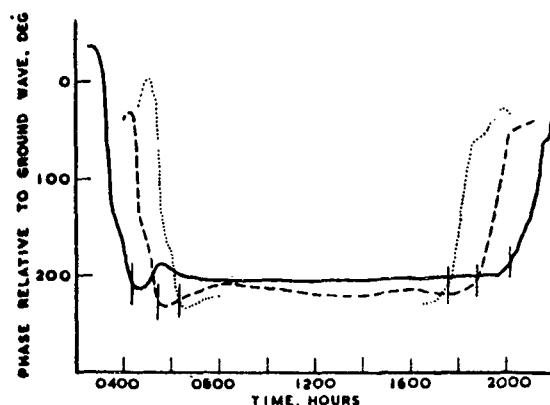
Fig. 15—Diurnal variation of phase of reflection on 16 kc/s at 540 km.

denotes times of sunrise and sunset

—— 2nd August, 1949.
- - - - 7th September, 1949.
. . . . . 5th October, 1949.

Fig. 16— Changes in apparent height of reflection, near sunrise, averaged over seven days in July, 1949.

. . . . At 71·14 kc/s.
+ + + + At 85·37 kc/s.
× × × × At 113·83 kc/s.

The arrow indicates the time of ground sunrise at the mid-point of the path.

Fig. 17—Experimental determination of reflection coefficients at various distances from the sender.

● — ● — ● At 85 kc/s. in winter.
— — + — + At 70·83 kc/s, in summer.
× — × — × At 85 kc/s, in summer.
▼ — ▼ — ▲ At 127·5 kc/s, in summer.
⊕ At 70·83 kc/s, in summer.
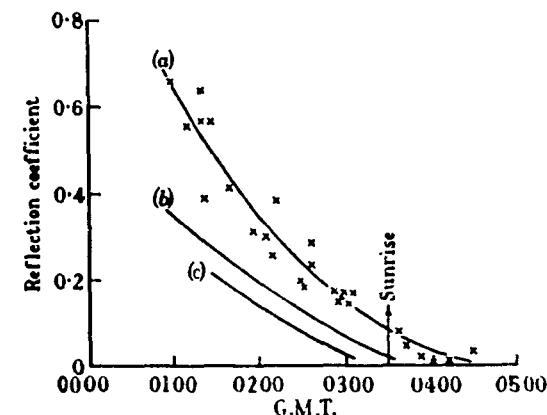
Fig. 18—Variation of reflection coefficient with time near sunrise; averages of seven days' observations during July, 1949.

× × × × All observed results at 71·14 kc/s.
(a) At 71·14 kc/s.
(b) At 85 kc/s.
(c) At 113·3 kc/s.

The arrow indicates the time of ground sunrise at the mid-point of the path.

66
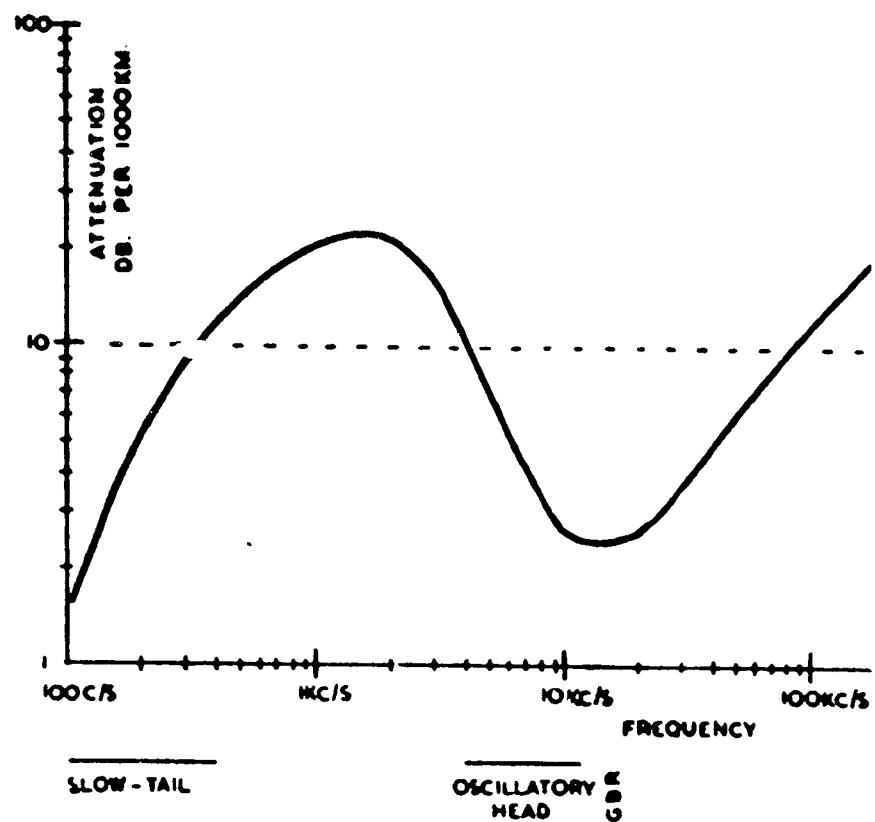
Fig. 19—Variation of attenuation
with frequency.

Fig. 22.—Changes in total signal and indicated phase difference at distances between 850 and 950 km from the senders, during a typical sudden ionospheric disturbance, 16 April 1950.

++++ At 71·14 kc/s.
×××× At 85·37 kc/s.
At 113·3 kc/s.

(a)
Relative amplitude
G.M.T.
1200   1300

(b)
Indicated phase difference, deg.
G.M.T.
1200   1300

Fig. 21.—The relation between the change of amplitude observed on 16 kc/s and the size of the phase anomaly during a sudden ionospheric disturbance. ΔA represents the maximum change in amplitude during the SID. Ā represents the mean amplitude before and after the SID.

Decrease of equivalent height, km
ΔA/Ā

Fig. 20.—A comparison between the changes of phase and amplitude observed during a sudden ionospheric disturbance on 16 kc/s (×), 70 kc/s (·), and 113 kc/s (×), on 7 October 1948.

(a)
Change of apparent height, km
G.M.T.
1530   1600   1630   1700

(b)
Conversion coefficient, ₙR₁
G.M.T.
1530   1600   1630   1700

Fig. 23— Eclipse anomaly obtained by subtracting mean of control days from eclipse day.
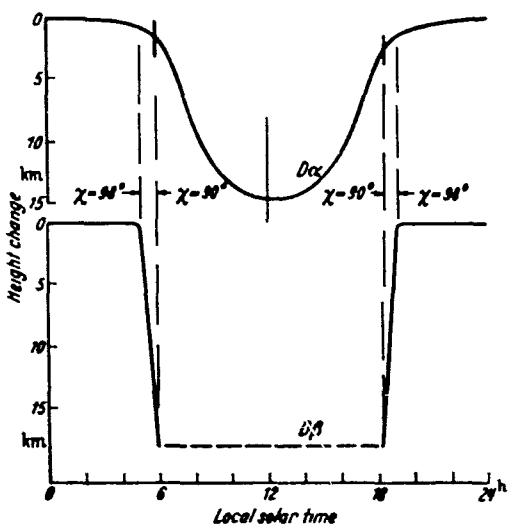
Fig. 24— The diurnal height variations of the layers $D\alpha$ and $D\beta$.

69
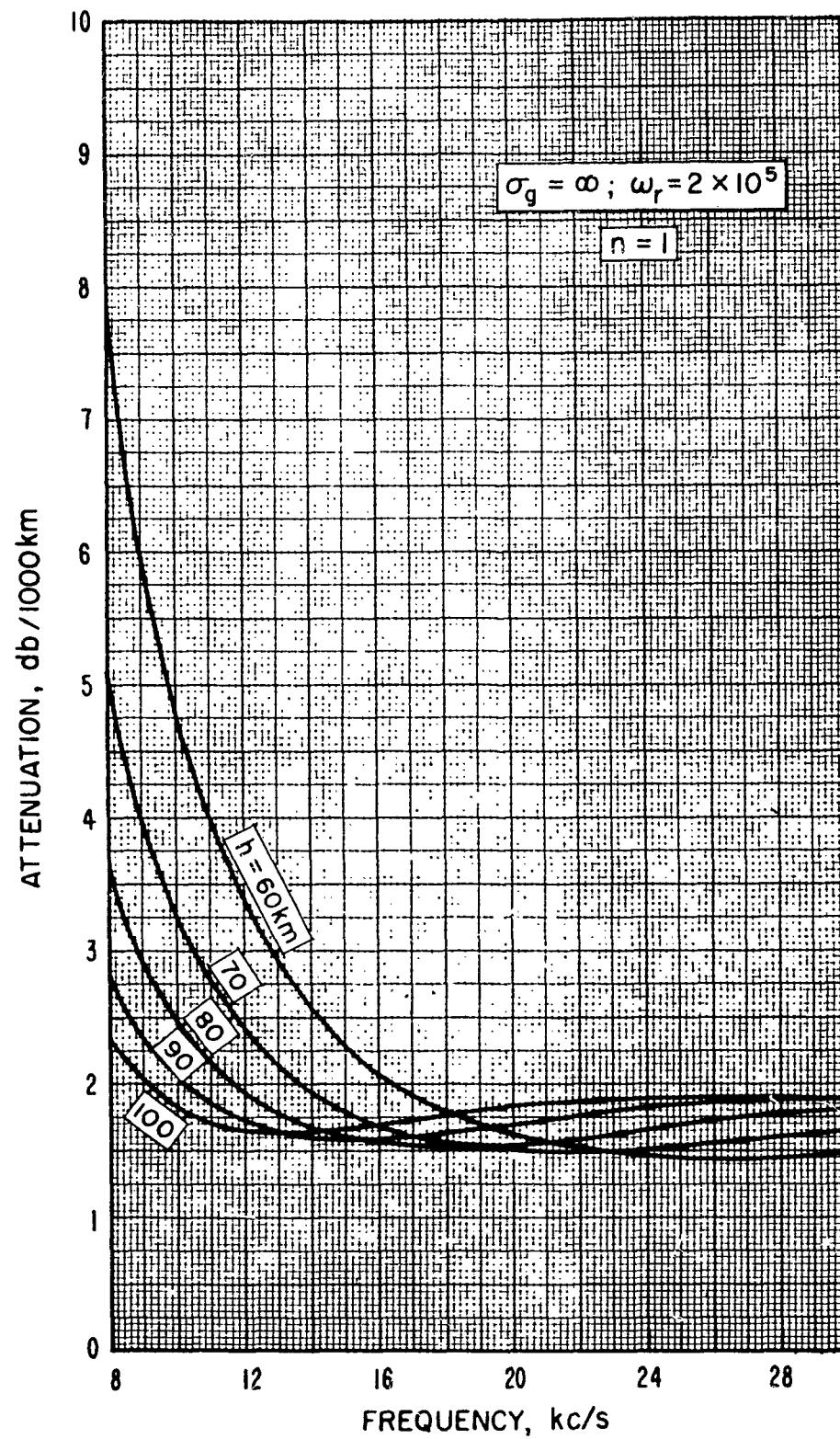
Fig. 25--Calculated attenuation vs. frequency for a
sharply bounded ionosphere of effective
conductivity $\omega_r = 2 \times 10^5$ for various heights.
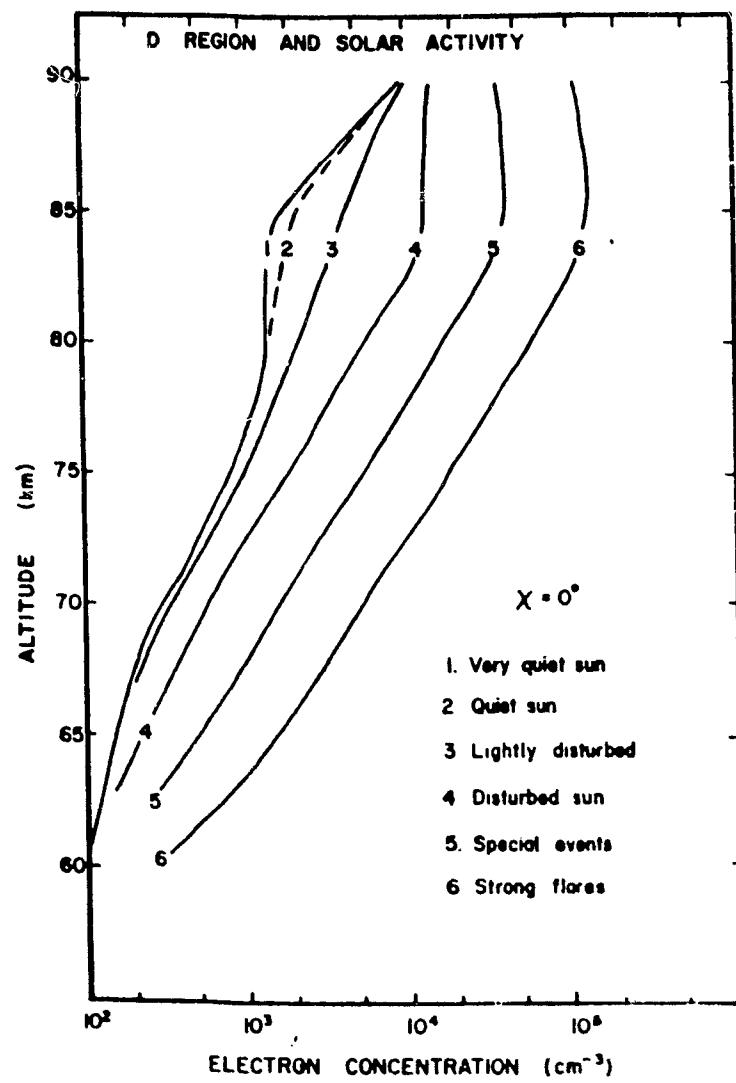
Fig. 26—Variation of electron concentration with height for various solar conditions.

71